NTNU – Trondheim
Norwegian University of
Science and Technology

Winding and Testing of Superconducting Coils

Jan Christian Eliassen

Master of Science in Electric Power Engineering
Submission date: June 2015
Supervisor: Arne Nysveen, ELKRAFT
Co-supervisor: Niklas Magnusson, SINTEF Energy

Norwegian University of Science and Technology
Department of Electric Power Engineering

Preface

This study is carried out at the Department of Electric Power Engineering, Norwegian University of Science and Technology during spring 2015

The subject is proposed by SINTEF Energy Research and is a part of a joint European project named INNWIND.EU, that is investigating a design of state of the art 10 - 20 MW offshore wind turbines.

I would like to thank my supervisor Professor Arne Nysveen at the Department of Electric Power Engineering, NTNU for his involvement during the project period.

Additional thanks to my supervisor from SINTEF Energy Research, Niklas Magnusson for his close collaboration in the lab and guidance throughout this project.

I also want to show my gratitude to the workers at the workshop at NTNU/ SINTEF who has been to a great assistance and provided quick deliveries. A thank to Ingulf Helland for his consultancy regarding soldering techniques. And last, a thank to Bård Almås at the servicelab at NTNU for his help during the project.

Trondheim, June 18, 2015

Jan Christian Eliassen

Problem Description

With the increasing power demand worldwide research on more cost-efficient energy production is inevitable. Superconducting rotor windings are considered for large offshore wind turbine generators to reduce size, weight and possibly costs.

This master thesis is a part of an ongoing research at SINTEF Energy, along with collaborates form a joint European project named INNWIND.EU. The thesis is a further development of the specialization project, "Methods for winding uninsulated superconductor coils with MgB_2". During the master project ten double pancake coil will be made. Without a specific turn-to-turn insulation the coils are cast by a wet winding technique and shaped as a racetrack. The winding method will be verified by testing the turn-to-turn insulation level. In addition the resistive and inductive parameters are to be determined under room temperature conditions.

A method for splicing MgB_2 sandwich conductors is to be developed and tested. A soldering tool will be custom designed for soldering such joints and verified by measuring the resistivity of these joints under superconducting conditions.

Project start-up:	January 2015
Supervisor:	Arne Nysveen, Department of Electric Power Engineering
	Niklas Magnusson, SINTEF Energy Research

Abstract

Superconducting rotor windings are considered for future large offshore wind turbines for their low weight, volume and their possibility to reduce costs. In a joint European project, INNWIND.EU, a superconducting small scale generator pole will be designed, build and tested. In this master thesis, the coil will be constructed out of ten sections, each consisting of a double pancake coil with 104 turns. These coils will be wound with a wet-winding technique, without a specific turn-to-turn insulation where the applied epoxy constitutes the insulating layer between turns. The insulating ability of the epoxy is validated by measuring the turn-to-turn resistance. Several test coils has been built, tested and investigated for possible internal contacts. The results indicate that the coil will not be damaged during normal operation, DC ramping or AC magnetic fields in the rotor windings. However, the winding method relies on the fabrication of the MgB_2 wire, where irregularities has been discovered on the wire which has caused an internal contact. A splicing procedure has been developed. A custom designed high power soldering tool has been constructed and joints are tested. The joints will produce approximately 1 - 5 mW during operation.

Sammendrag

Superledende rotorviklinger vurderes for framtidig bruk i store offshore vind turbiner på grunn av deres lave vekt og volum, samt muligheten for å redusere kostnader. I et felles samarbeid under navnet INNWIND.EU, skal en nedskalert superledende generator pol designes, bygges og testes. I denne avhandlingen vil spolen bli bygget av ti mindre seksjoner, hvor hver seksjon består av en dobbel pannekake vikling med 104 vindinger. Disse spolene vil bli viklet med en våt-vinding uten en spesifikk vindings isolasjon, hvor den påførte Epoxyen utgjør isoleringen. Isolasjonsevnen til Epoxy skal valideres ved å måle vindingsresistansen i spolen. Flere testvikklinger har blitt bygget, testet og undersøkt med tanke på mulige interne kontakter. Resultatene indikerer at spolen ikke vil ta skade under normale DC operasjoner, DC sprang eller AC magnetiske felt i rotor viklingene. Imidlertid så er viklemetoden avhengig av fabrikasjonskvaliteten av MgB_2 lederen, hvor uregelmessigheter på strømlederen har blitt oppdaget som har forsaket en intern kontakt i spolen. En metode for å skjøte superlederen har blitt utviklet. Et spesialbygd høyeffekts loddeverktøy har blitt konstruert og skjøtene har blitt testet. Disse skjøtene vil produser ca. 1 - 5 mW under drift.

Contents

List of Abbreviation

AC	Alternating Current
DC	Direct Current
HTS	High Temperature Superconductor
LTS	Low Temperature Superconductor
PIT	Powder In Tube
T_C	Critical Temperature

List of Tables

List of Figures

Chapter 1

Introduction

1.1 Background

To address the climate change, the EU member states have decided to reduce 20 % of greenhouse gas emissions by 2020 compared to the 1990 level. The energy consumption should be reduced by 20 % and 20 % of the energy demand should be supplied by renewable energy. One of the main technologies considered to this demand is wind power [1].

> The December 2008 agreement on the 2009 Renewable Energy Directive[...]The directive sets binding national targets for the share of renewable energy in each of the 27 EU Member States in 2020[...] It is by far the most significant legislative effort to promote renewable energy, including wind power, any-where in the world. [2, p.47]

By 2020 the wind power capacity is forecast at 213 GW, where 43 GW is constituted by offshore wind power. The wind energy will produce 495 TW h and is assumed to reduce CO_2 emissions by 0.588 Mt CO_2/TW h. In 2020, wind power is forecast to produce 14 % of Europe's total electricity consumption [2].

Today the average wind turbine size installed is 3,0 - 3,6 MW. Some 5 MW will be produced, and further development of the turbines will be expected since the turbine cost represent about half of the total installation costs. However, the turbine size is dependant of local water and wind conditions. An estimate done by the developer of the UPWIND project indicates that a 10 MW turbine will be desirable. Land based installations would probably not increase from today's 3 - 3.6 MW turbines due to transport limitations [1].

1.2 Superconducting Wind Turbine Generators

Superconducting rotor windings are considered for large offshore wind turbines due to their advantage of low weight, volume and their possibility to reduce costs. The volume and weight is magnetic field dependant as

$$P = \omega\tau \tag{1.1}$$

where, P is the power, ω the angular frequency given by maximum tip speed and τ the torque. The torque is given by

$$\tau \propto BIV \tag{1.2}$$

where B is the air gap magnetic field, I the stator current and V the generator volume. The only variables to change are the magnetic field strength and the volume. In comparison, a superconductor generator volume is 40 % less than a corresponding permanent magnet [3]. In addition, the turbine design can be simplified because of this weight and volume reduction. It may be advantageous to omit the gearbox by utilizing a multi-pole generator which is driven directly by the turbine rotor [4]. For offshore installations the reliability is a crucial factor and the most frequent operational errors relate to bearing and gearbox failures [1]. In the North Sea, there are offshore location, only accessible six months out of the year. Reduction in major repairs can change the cost of energy significantly [5].

"Cost is both the prime concern and the prime driver." [3, p.16]

For generator rotor windings several types of superconductors are considered. Both High-Temperature and Low-Temperature superconductors are represented in this selection. The operating temperature, magnetic field strength, cost and availability are all factors which inflict the choice of superconductor type. There are several actors with different concepts, developing generator design, e.g. General Electric, AMSC and INNWIND.EU. The represented superconductors are $NbTi$, $YBCO$ and MgB_2 respectively [3]. For offshore wind farms, the cost of foundations and connections can amount to 70 % of the first cost. Larger wind turbines would reduce these costs. [5]

"In the end, it is all about costs." [3, p.2]

Chapter 2

Superconductivity

Introduction

This chapter gives an introduction to the phenomenon of superconductivity with its remarkable properties and accompanying limitations. First a brief review of the history is presented followed by some details regarding the properties and limitation. Then an introduction to the MgB_2 superconductor used in this project is given.

2.1 History

The discovery of superconductivity was a outcome of Helium liquefaction achieved by Heike Kamerling Onnes. At Leiden institute, Onnes used the Linde technique and achieved as first person ever to liquefy helium in 1908. This was the turning point for the entire condensed matter physics community. Heike Kamerlingh Onnes achievements of liquefying helium were rewarded with The Nobel Prize in 1913.

Kamerlingh Onnes studied the properties of materials at low temperatures. He investigated the conjectures that the electrical resistivity would become zero or behave unexpectedly, such as reaching a minimum and then rise again, as temperatures approached absolute zero. He carried out electrical resistivity measurements on pure platinum and gold and discovered that the resistivity reached a constant value, independent of temperature below 10 K. However, the purity of the metal affected the resistivity and purer metal attained lower resistance. Therefore, he investigated mercury, which has the property to become ultra-pure through multiple distillations. The resistance suddenly and unexpectedly dropped to zero just below 4.2 K and

Kamerlingh Onnes discovers superconductivity, in 1911. Later on Kamerlingh Onnes found more metals, which shared this phenomenon and thereby concluded that the purity of mercury did not affect the superconductive property, as lead and tin had also become superconductive at 7,2 K and 3,7 K respectively.

Leiden Laboratory was the center for condensed matter physics until low temperature research began to spread around 1934-35. The first commercial helium liquefier, ADL Collins Helium Cryostat, built by Samuel Collins at Massachusetts Institute of Technology in 1946 made the condensed matter physics to flourish worldwide. More elements where discovered to contain superconducting abilities, however, they all shared a common disappointment with low T_C values. In addition, it is not discovered a rule to which elements that would become superconducting. Characteristic parameters such as melting point or crystal structure did not reveal any trend to which metals who would possess superconducting abilities. Due to the disappointing properties, scientist changed track and started to look for superconducting abilities in alloys and compounds. Superconductivity was indeed discovered in a large number of alloys and compounds.

In 1986, Alex Müller and Georg Bednorz made a breakthrough in the field of superconductivity as they discovered superconductivity at highest temperature then known at 30 K. Even more noteworthy is that they found superconductivity in a brittle of ceramic, which are commonly used as insulators, thus they do not conduct electricity well at all. This discovery awarded the two men with The Nobel Prize in 1987. As ceramics revealed superconductivity at much higher temperatures, scientist found in 1987 the first superconducting material above temperatures of liquid nitrogen. Superconductors who enter superconducting state at the temperature of liquid nitrogen is known as high-temperature superconductors (HTC) while superconductors who operate at the temperature of liquefied helium is referred to as low-temperature superconductors (LTS). In Figure 2.1 a selection of superconductors are displayed with respect to year of discovery and critical temperature.

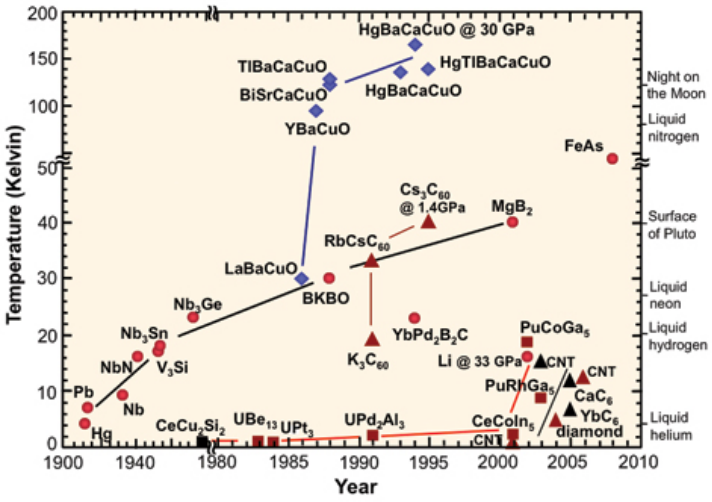

Figure 2.1: Discoveries of superconductors through history and coherent critical temperature(Courtesy Coalition for the Commercial Application of Superconductors).

2.2 Superconducting Properties and Limitations

Heike Kamerlingh Onnes first discovered superconducting state in pure mercury at liquid helium temperature in 1911. He also discovered that the superconducting state is not only dependent on the temperature. When he injected his sample of superconducting lead with a current of only 4.2 A mm^{-2} the potential difference was no longer zero and beyond this threshold of current it would rise rapidly and the lead would leave the superconducting state. Kamerling Onnes also observed that his sample would exceed superconducting state when exposed to a magnetic field of 60 mT. Thereby stating that superconducting material can only become superconducting when these critical values of temperature (T_C), current density (J_C) and magnetic field (B_C) are met. They form a inter-dependant surface known as critical surface as shown in Figure 2.2 [6].

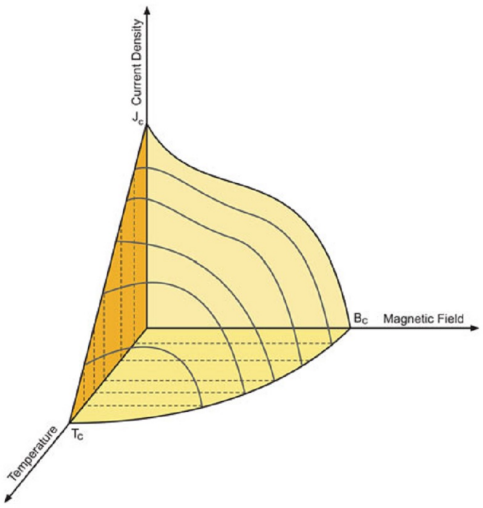

Figure 2.2: Critical surface of a superconductor [6].

In superconducting state, the resistivity vanishes and a perfect conductor will not sustain an electric field, meaning that E=0. Maxwell Equations, and more specific Faraday's law;

$$\nabla \times E = -\frac{\partial B}{\partial t}, \tag{2.1}$$

$$E = 0 \Rightarrow \frac{\partial B}{\partial t} = 0 \tag{2.2}$$

implies that the magnetic flux inside a superconductor should be constant. This means that if a superconductor is exposed of magnetic flux and then cooled below T_C (the electric field strength becomes zero, ∂B becomes zero) the magnetic flux should be trapped inside the superconductor, although the magnetic field is removed. This is not what Walter Meissner and Robert Ochsenfeld observed when they studied superconductors in 1933. Instead of the expected behavior as described, they discovered that the magnetic flux was repelled from the superconductor the moment it entered superconducting state, regardless if the superconductor was exposed to a magnetic field before or after reaching superconducting state. This effect is named the Meissner effect and is unlike the behavior of a normal metal, a superconductor becomes a perfect diamagnet in superconducting state. When an external magnetic field is applied, screening currents are induced on the surface of the superconductor (with a penetration depth of approximately λ = 10-100 nm) which cancels out the magnetic flux, hence B=0 inside a superconductor. The Meissner Effect is illustrated in Figure 2.3a.

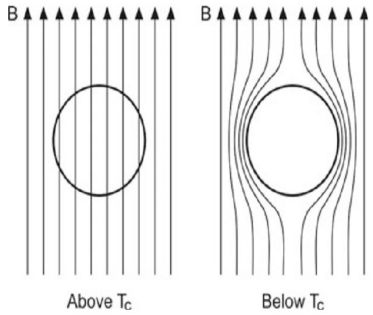

(a) Illustration of Meissner effect and how the magnet flux is repelled from the body of the superconductor[6].

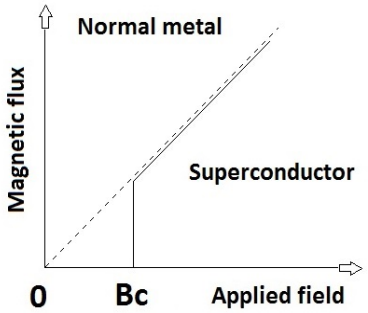

(b) Magnetic flux distribution inside a superconductor when an external magnetic field is present.

Figure 2.3: Illustration of The Meissner effect and how the magnetic flux is changed inside the superconductor for temperatures above and below the critical temperature and critical magnetic field.

2.3 Type I and Type II Superconductor

As mentioned, superconductors are categorized by their transition temperature, either as HTC or LTC . In addition, superconductors are also categorized by how they repel an external magnetic field. Type I superconductors are perfect diamagnets in superconductive state, as presented in Figure 2.4a, while type II superconductors show perfect diamagntism up to a lower critical field, B_{C1}, and then enters a mixed state where it allows partial flux penetrations known as vortices, as shown in Figure 2.4b. These vortices are small, normal, tube-like regions inside the superconductor with a specific amount of flux, a flux quantum, Φ_0. The value of the flux quantum is

$$\Phi_0 = \frac{h}{2e} = 2.07 \times 10^{-15} \quad [Vs], \tag{2.3}$$

where h is the Planck constant and e is the electron charge. The superconductor leaves the mixed state and become normal when B exceeds B_{C2}.

During the mixed state of type II superconductors, high current may be transported under high magnetic field, unlike type I. For this reason only type II superconductors are applicable for magnet constructions.

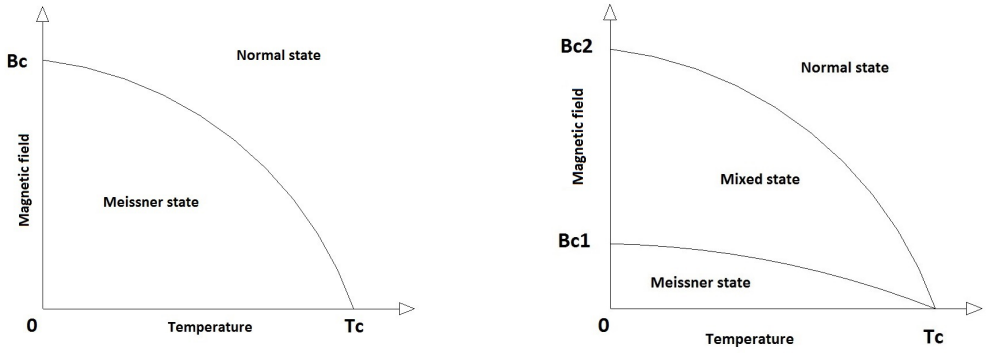

(a) Type I superconductor.

(b) Type II superconductor.

Figure 2.4: Magnetic phase diagrams for superconductors type I and type II.

2.3.1 The Mixed State

In the mixed state, impurities in the superconductor allow for penetration of vortexes. When a longitudinal current flows through the superconductor, the vortices experience a Lorentz-like force as illustrated in Figure 2.5.

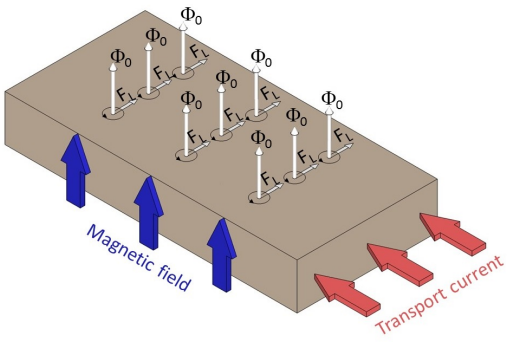

Figure 2.5: Illustration of the penetration of vortices and the Lorentz-forces when a transport current is present

This force per unit length can be written

$$f_L = J \times \Phi_0 \,, \tag{2.4}$$

where J is the transport current and Φ_0 is the vector form of the flux quantum pointing along the flux line. These forces act on the vortices and make them move when they exceed a pinning force f_P, set up by structural defects in the superconductor. Hence, vortices start to move perpendicular to their axes and the transport current when $f_P \leq f_L$. This movement induces an electric

field

$$E = B \times v \,, \tag{2.5}$$

where B is the magnetic field corresponding to the density of vortices and v is the average velocity of the vortices. This induced voltage is the key to determine the critical current $\mathrm{I_C}$, and for a given temperature and magnetic field, the current is at a critical value when the electric field along the conductor reach $1\,\mu\mathrm{V\,cm^{-1}}$, as shown in Figure 2.7. Hence, the critical current is dependant of the structural defects and its ability to oppose the movement of vortices, as illustrated in Figure 2.6.

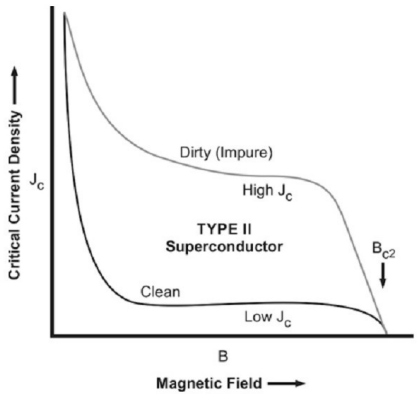

Figure 2.6: Illustration of how J_c is affected of the purity of the superconductor in the current versus magnetic phase diagram [6].

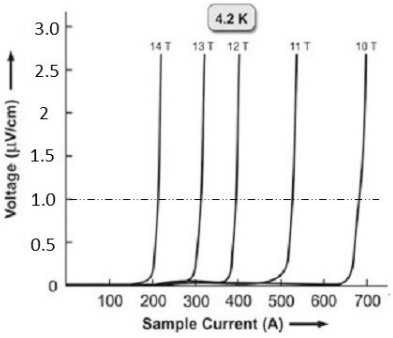

Figure 2.7: Voltage characteristics for a superconductor when critical current $\mathrm{I_C}$, is passing though under different external magnetic fields [6].

When the motion of vortices enforce an electric field, and since the transport current are not perpendicular to this induced voltage, power is dissipated. The power loss per unit volume is given by

$$P = E \cdot J \,. \tag{2.6}$$

This generated power must be removed by the cooling device. The amount of energy needed to remove one Watt energy at the operating temperature of the superconductor is denoted the cooling penalty factor n_{cp}, which is determined by the carnot factor η_{carnot} and the efficiency of the cooling device, $\eta_{cooling}$, in the following way:

$$n_{cp} = \eta_{carnot} \cdot \frac{1}{\eta_{cooling}}. \tag{2.7}$$

The carnot factor is denoted by how many Watts needed to remove one Watt of generated energy in an ideal cooling machine at low temperature:

$$\eta_{carnot} = \frac{T_{amb} - T_{low}}{T_{low}} \tag{2.8}$$

where T_{amb} is the ambient temperature and T_{low} is the operating temperature of the superconductor.

2.4 MgB_2 Superconductor

Japanese scientist discovered in 2001 the superconducting ability in the binary compound magnesium diborid, MgB_2. This new superconductor had significantly higher T_C than other conventional metallic superconductors. As shown in Figure 2.8 there is a sharp transition to the superconducting state at 39 K. The superconducting sample consisting of a magnesium-to-boron ratio of 1:2 were prepared from powdered magnesium (99,9% pure) and powdered amorphous boron (99% pure) in a dry box. The powders were mixed, grounded and pressed into pellets and heated in a hot isostatic furnace to 973 K for 10 hours under high argon pressure (196 MPa) [7].

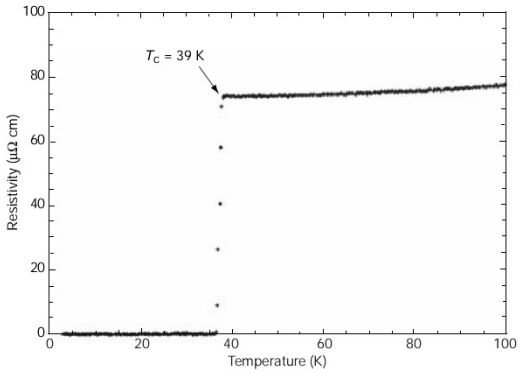

Figure 2.8: Resistivity versus temperature plot of a MgB_2 superconductor under zero magnetic field [7].

In addition to the relatively high T_C and its advantage of avoiding the use of hazardous liquid helium, the MgB_2 is cheap compared to HTS cuprates which contain up to 70% Ag [6]. The fabrication of MgB_2 can be conducted by either powder in tube technique (PIT) or a coating technique. The coating technique use a hastelloy coated with MgB_2 to provide tapes with superior quality. However, when producing long lengths the PIT technique is ideal. The PIT technique involves rolling of well-prepared fine powder packed at

high density into a fine size of wires or tapes. To maintain ductility, the process contains a series of rolling and intermediate annealing. Both techniques provide a stabilized multi-filamentary wire or tape suitable for magnet applications.

The MgB_2 filaments need both mechanical and thermal support when implemented into a wire. This is done by adding a cladding material to the filaments. This material must not react with the magnesium diborid filaments, and amongst several suited metals Fe, Ni and stainless steel turns out to be the best cladding materials. However, copper has to be incorporated for thermal stability [6].

2.4.1 Superconductor Properties from Columbus Superconductors

The superconductor used in this project is delivered from Columbus superconductors and this section gives a brief summary of properties of the magnesium diboride superconductor.

Wire Format and Dimensions

The sandwich MgB_2 wire is a multi-filament with 19 filaments. These filaments are embedded to a nickel sheet and constitutes 21.5 % of the nickel cross-section of 1.5 mm^2. The total wire cross-section is 3 mm $\times$ 0.7 mm, where the nickel and the external copper stabilizer height is 0.5 mm and 0.2 mm respectively. The wire cross-section is shown in Figure 2.9.

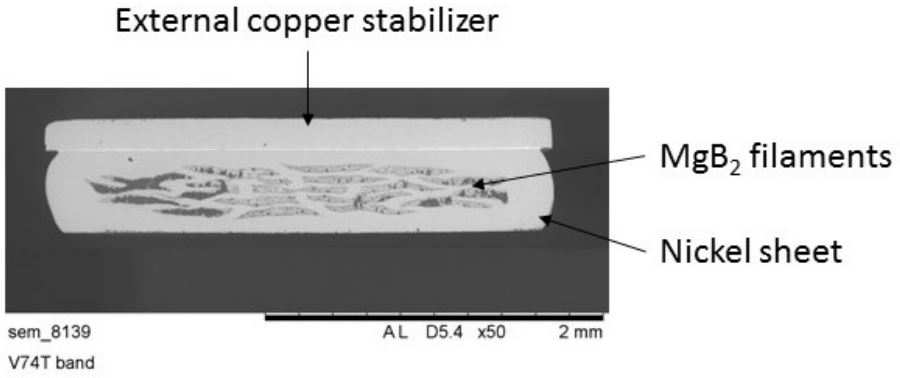

Figure 2.9: Cross-section of MgB_2 wire(Courtesy Columbus Superconductors).

Mechanical Properties

The superconductor is fragile and must be treated carefully. If bended with lower bending radius than stated in Figure 2.10 a degradation of critical current occurs. The minimum bending radius is 150 mm when the copper stabilizer is facing outwards, and 350 mm when it is facing inwards. In addition, tensile strain can damage the wire if it exceeds approximately 115 MPa, as shown in Figure 2.11.

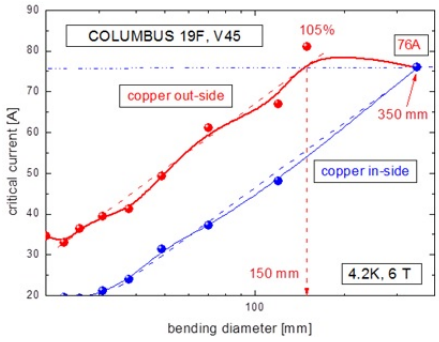

Figure 2.10: Critical current versus bending diameter.

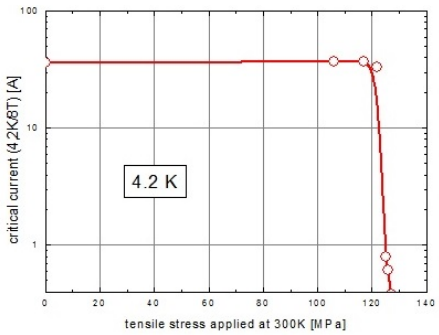

Figure 2.11: Critical current versus tensile stress.

Critical Current

The critical current is varying from batch to batch. This originates from purity of the elements used in each batch. The superconductors which are delivered for this project are identified by batch number. The critical current for each batch are given in Table 2.1.

Table 2.1: Critical current for delivered MgB_2 at 20 K and 1 T.

Batch	V1893	V1922	V1934	V1935	V1936
I_c[A]	472	486	452	N.A.	465

Chapter 3

Winding Procedure

Introduction

The MgB_2 superconducting tape has been wound into a coil by the use of a wet winding technique. This coil is build up of ten sections of double pancake coils in the shape of a race track, with a straight section of 0.5 m and a circular section with radius of 0.15 m, as shown in Figure 3.1. Approximately 455 m of tape has been used to wind the 104 turns of each layer.

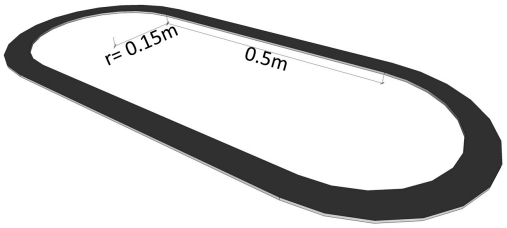

Figure 3.1: Double pancake coil with dimensions.

Winding a double pancake coil requires a lot of preparation, careful execution and finalization. It is a time consuming process, where experience is a decisive factor. A custom-made winding table has been built at SINTEF Energy, covering all requirements to prepare and wind a complete double pancake coil. This winding table can be set up either vertical (Figure 3.2) or horizontal (Figure 3.3) for the requisite tasks of preparation and execution respectively.

3.1 Preparation

The MgB_2 superconductor is delivered by Columbus Superconductors on cable drums with a length of either 500 m or 2000 m. These cable drums are unsuitable for winding and therefore, the superconductor is first wound from factory drums onto special cable discs. When doing this the cable drums are mounted onto a pole for unwinding as indicated in Figure 3.2. While winding the required amount of 500 m from factory drums onto cable disc, the tape should pass through a device which measure the length. However, due to complications it had to be excluded. Nevertheless, during previous windings there were made marks on the cable discs, to indicate the distance at each fifty meter. These marks will be sufficient to measure the tape, as it is about 30-40 meters excess tape from each coil.

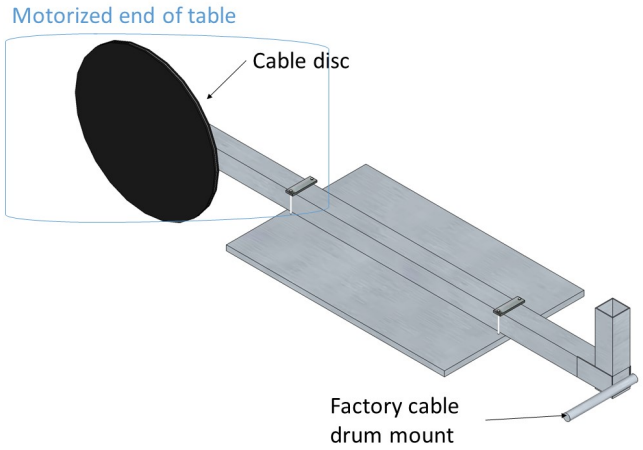

Figure 3.2: Description of winding table in the vertical position.

When the sufficient length of superconductor is wound onto the cable disc, the winding table can be turned to a horizontal position. The mold is then placed at the motorized end of the table. This mold is smeared with Emerson & Cuming mold release 122 S to ease the removal of the coil when the epoxy has hardened. Placement barriers are attached to the mold to ensure that the superconducting tape is placed in a correct manner. This is shown in Figure 3.3.

A double pancake coil is wound by starting at the middle of the wire where one half is used for the lower layer and the other half of the upper layer. Therefore, half of the conductor needs to be wound onto a second cable disc. This cable disc is placed on top of the mold before the tape is wound onto it as illustrated in Figure 3.4. Again the marks on the cabledisc is used to locate the middle (roughly) of the superconductor.

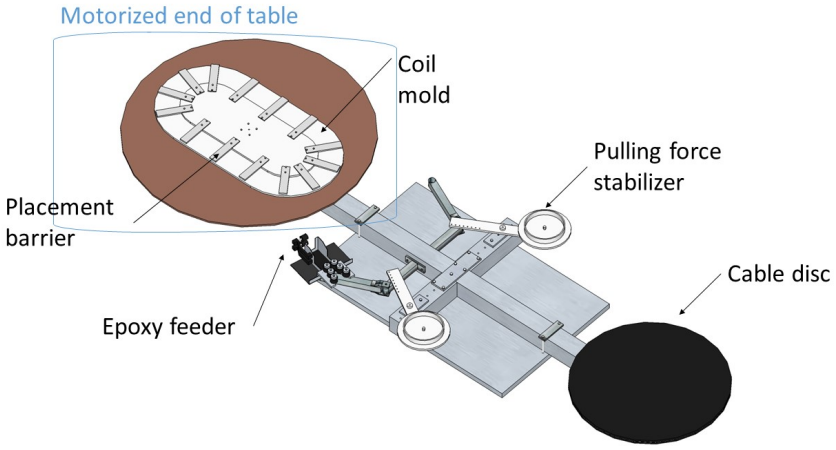

Figure 3.3: Description of winding table in the horizontal position.

When the sufficient length of superconductor is wound onto the second cable disc and the mold is in the correct rotational position, such as in Figure 3.4, the cable disc is carefully moved further back along the winding table. This is done to minimize tension when the tape is lowered to its correct position for winding the first layer. The table is a pulling table, which means that one side has an engine and the other has a break. This break is adjusted so that the pulling force is approximately equal to tensile stress of 20 MPa. A counter is mounted underneath the rotating mold to keep track of the number of turns.

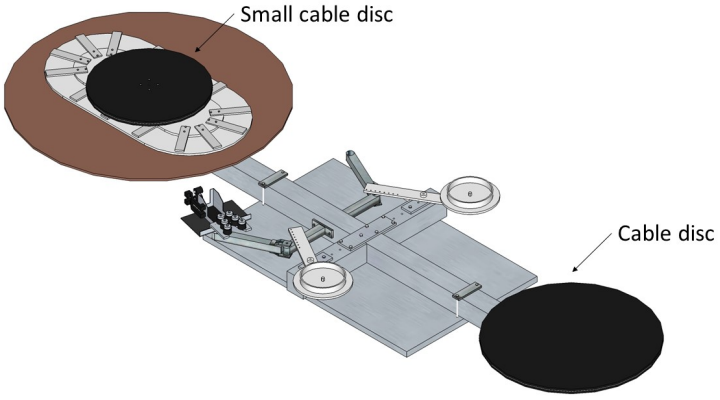

Figure 3.4: Winding table with attached cable discs.

3.2 Winding the Lower Layer

The winding of the first layer can begin when proper preparation is done. The winding process starts with the mixing of alumina filled Epoxy Stycast 2850 and hardener catalyst 24LV (weight-ratio = 1:0.06). The composition must be mixed properly, normally it takes approximately 5 minutes. Then the epoxy feeder must be placed carefully without damaging the conductor. This is a two person job and therefore not a part of the preparation. As the superconductor is in place inside the epoxy container, the epoxy is poured into it. Then the winding can commence. In the beginning, the winding speed is very slow and multiple stops are required to get a controlled transition between upper and lower layer (as a double pancake starts on the middle with this transition), and adjust the proper tape height to avoid risk of the tape shall get hung up. When the tape settles nicely, the speed is increased. At this stage the only necessity is to make certain that the epoxy container does not run out of epoxy. Nevertheless, the process is carefully monitored in case of irregularity occur. The winding speed is reduced as the last turn of the lower layer is approaching. The tape is then cut and attached onto the table in such way that it is not damaged nor in the way for winding of upper layer.

3.3 Intermediate Winding Stage

The first layer of the double pancake coil is wound, and some intermediate preparations are necessary before winding the upper layer, thus complete the coil. The second cable disc has to be carefully moved from the mold onto the opposite end of the table. This is a process which easily can damage the superconductor if done without caution. However, when the cable disc is removed and the mold is available for adjustments, the placement barriers can be removed. The superconductor is then pressed towards center on the straight sections to maintain the desired dimensions. If the appliance of epoxy had been to generous, excess epoxy had been removed. To avoid the risk of flash over between upper and lower layer, shim plates made of stiff epoxy is evenly distributed on top of the lower layer as shown in Figure 3.5. The placement barriers have different height dependant of which way they are mounted and therefore, when producing the upper layer they need to be turned upside down. The second batch of epoxy is mixed when the counter is reset, the epoxy feeder is placed on the opposite side and motor connection has changed polarity as the winding table need to change rotating direction when winding the upper layer.

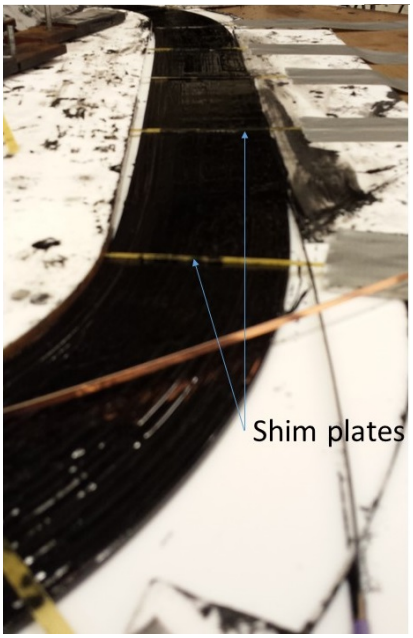

Figure 3.5: Distribution of shim plates.

3.4 Winding the Upper Layer

For the first meter of the upper layer the epoxy is needed to be applied manually, since this part of the tape is unable to pass through the epoxy feeder. As with the lower layer, the winding starts at a slow winding speed with multiple stops to adjust the proper tape height to avoid that the superconductor may be hung up. Due to the multiple shim plates, the risk is significantly higher at this stage. As the tape settles nicely, the speed is increased. Again as with the first layer the only necessity is to make certain that the epoxy container does not run out of epoxy. Nevertheless, the process is carefully monitored in case of irregularity occur. The winding speed is reduced as the last turn of the upper layer is approaching. When the last turn is almost completed, the winding is stopped. The epoxy feeder is removed (carefully) to avoid appliance of epoxy at the end of the tape. When the upper layer is completely wound, only the finalization remains. Placement barriers are removed and the pressure plates holding the lower layer in place is replaced with a higher pressure plate (Appendix B.5). This pressure plate apply pressure evenly on both layers and are pressed towards center until the width of the coil section is 84 mm. A small length of superconductor is dipped in epoxy and attached to the outgoing connections for mechanical support, since this is the weakest points of the coil. To ensure that the turns does not have

any height deviations, downwards pressure is manually applied on top of the shim plates to even out any irregularities. Excess epoxy is removed before adding a mold that fits on top of the coil. Weights are added for downwards pressure and the coil is stored over night for hardening. The equipment is then disassembled and the coil is carefully removed from the mold, inspected for damages and placed onto the thermal interface as shown in Figure 3.6.

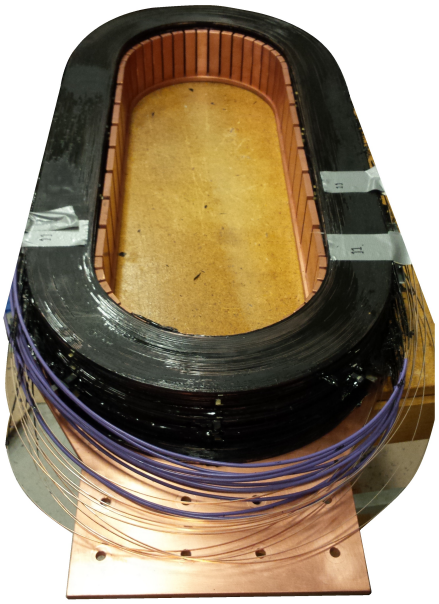

Figure 3.6: Stacked superconductors onto thermal interface.

Chapter 4

Test coils

Introduction

In a previous test coil made during the specialization project, "Methods for winding uninsulated superconductor coils with MgB_2" [8], it was discovered deficiencies that must be set in order to accomplish a satisfactory means to wound a double pancake coil. Mainly two problems are of interest, the deviations amongst turns in the upper layer and the variation of appliance of epoxy. Adjustments has been made to the equipment and additional test coils has been wound to confirm that the changes had improved the result.

4.1 Small Scale Test Winding

Previous experiences regarding wet-winding technique of a double pancake winding without specific turn-to-turn insulation, revealed the importance of proper application of epoxy. Therefore, some changes have been made to the epoxy container on the epoxy feeder (Figure 4.1). To reduce the amount of epoxy attached to the outgoing superconductor the front foam wall has been replaced with a harder type of foam. A smaller coil was built to test if the adjustments had improved the winding technique. During winding the amount of epoxy as expected, had been reduced and thus made the winding process easier. In addition, a more active use of height adjustments on the foam rollers had been applied, to minimize height deviations amongst the upper layer. This had a positive effect on the alignment and a comparison is displayed in Figure 4.2a and 4.2b. Nevertheless, some irregularity occurred on two spots along the opposite parts of the coil as illustrated in Figure 4.2c. This may arise from tension relief when the winding table turns around the circular section.

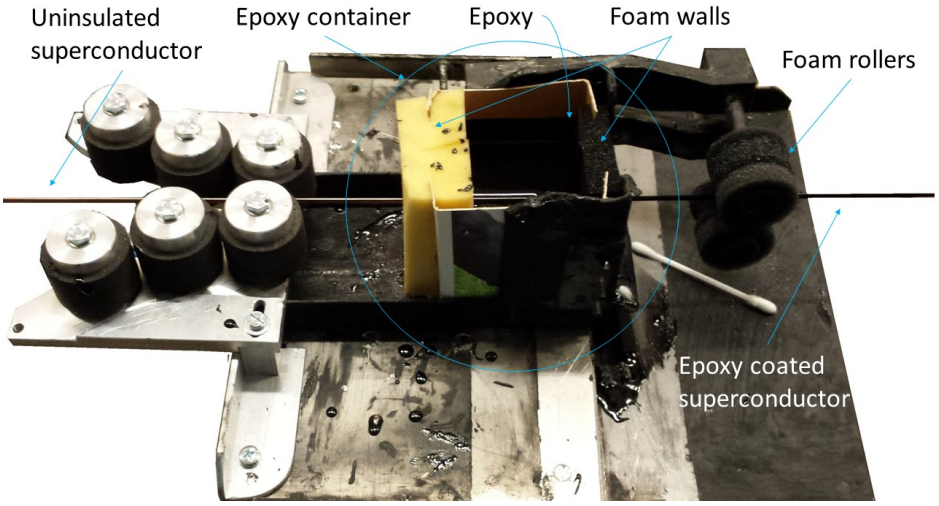

Figure 4.1: Epoxy feeder.

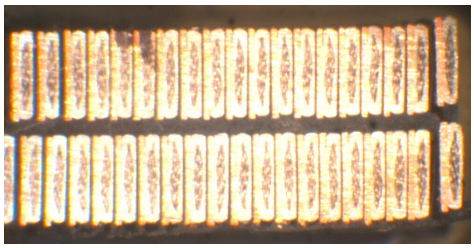

(a) Alignment of 20 turn test winding.

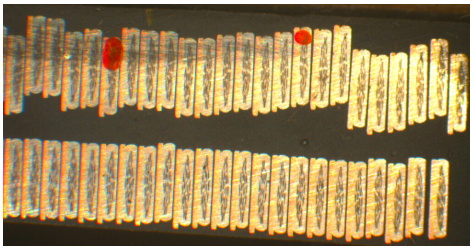

(b) Alignment of early test winding.

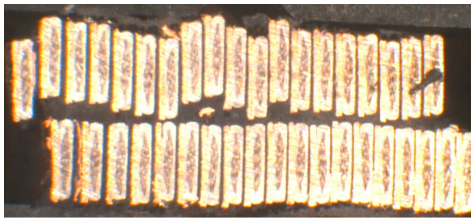

(c) Bad alignment 20 turn test winding.

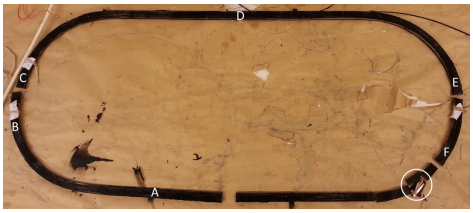

(d) Test coil and respective cuts.

Figure 4.2: Visual display of small scale test winding and comparison to previous work.

4.1.1 Insulation Test

To conclude that the new adjustments to the epoxy feeder did not bear upon the insulating ability of the epoxy, some test was conducted. The test coil was first energized by a DC current of 1 A in room temperature conditions, to measure the voltage distribution of certain parts of the coil. This may

indicate if there is contacts amongst turns or between the two layers. Further on the coil were cut into two parts, sanded and tested. Resistance was measured between each turn with a fluke multimeter and for lower values the four probe technique was used to determine the resistivity. The lowest values, typically below a couple of Ω (<5) may originate from uneven sanding, and these potentially surface contacts can have a very small size and are generally determined by

$$d = \frac{\rho}{R} \tag{4.1}$$

where d is the diameter of the contact, ρ is the resistivity of the contact material and R is the contact resistance. For a contact resistance of 5 Ω and resistivity 1.68×10^{-8} Ω m the diameter would be approximately 3.36 nm. This is not detectable in a microscope and therefore, an attempt of scorching the possible contacts were made by applying 10 V between the respective turns. This procedure had a positive effect on all except but one turn-to-turn contact. This is an indication that the contact is not on the cut surface, hence it must be inside the coil.

An attempt to locate the contact inside the coil was made by the use of the four probe measuring technique. The procedure used for locating the contact contains two steps. First, a current was injected through the contact and the potential was measured across it, as illustrated in Figure 4.3a. This method excludes the voltage drop across the superconductor from the measurement probes towards the contact, hence only the voltage across the contact is measured. Second, the electric potential drop across the superconductor prior to the contact is included as the electromotive force is measured at the same end as the current is injected, as illustrated in Figure 4.3b.

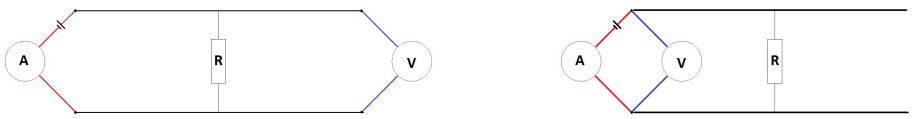

(a) Standard four probe measurement technique.

(b) Variant of four probe measurement technique.

Figure 4.3: Method to determinate distance towards contact.

As the voltage drop across the path prior the contact and the voltage across the contact is known, it is possible to locate the distance to the contact. However, due to unstable measurements this procedure failed. Therefore, it was necessary to further divide the test object to decrease the section that contains the contact. Figure 4.2d shows the entire test coil, all the cuts made

and the red circle indicates which part contains the contact.
The section of interest, now only a few cm long were dismantled and closer studies under a microscope revealed that a silver coloured tip had penetrated the epoxy and made contact with the neighbors turn. Estimated height of the tip is 4 µm. The tip is displayed in Figure 4.4a and 4.4b. In Figure 4.4b it is possible to see that the tip cast a small shade on the left hand side, which reveals that it is in fact a tip and not just a spot that lack epoxy. The tip might originate either by contaminations while winding the coil or from imperfection during fabrication of the superconductor. The latter is most probably the case, because the tip did not penetrate the epoxy, as it arose from a spot that lacked epoxy. If it were metal rest that had joined the mix of epoxy, it would have been the epoxy who glued it in between the two turns. As Figure 4.4b shows, the tip is not penetrating the epoxy and thereby must be attached to the superconductor. The resistivity of this contact where 46 mΩ.

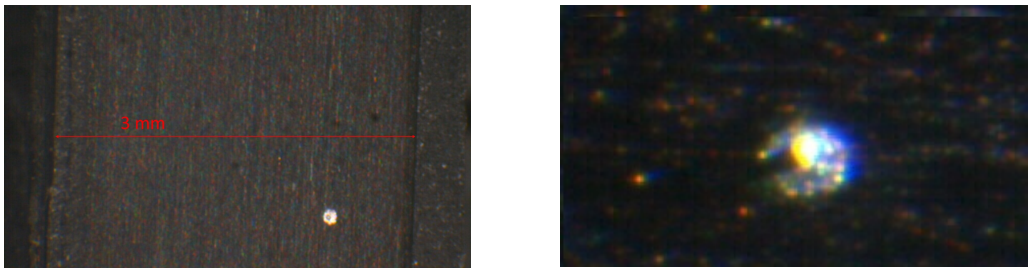

(a) Contact point (silver point). (b) Contact point with shade.

Figure 4.4: Snapshot taken of contact point through a microscope

4.2 Full Scale Test Winding

A full coil, consisting of 102 turns in each of the two layers in the double pancake coil, was made to confirm that the winding process and skills of the workers were sufficient to produce a flawless coil. For this coil approximately 500 m of MgB_2 superconducting wire were used combined with 1538 g of epoxy Stycast 2850 and 107.6 g of hardener catalyst 24LV.

As mentioned, in previous coils, the alignment of the upper layer had not been satisfying. Therefore, while winding the upper layer of the double pancake, the process was stopped at approximately every twentieth turn. Pressure (downwards on top of the location of shim plates) was added to smooth out any height deviations amongst the turns before continuing winding. In addition, instead of a uniform downwards pressure along the whole

length of the coil, pressure was added to the circular section of the coil while the epoxy was hardening. This was done by adding press plates at the desired locations. The press plates, were made of metal and smeared with a release agent. This was very inefficient as the press plates were not removable after the epoxy had hardened, as shown in Figure 4.5. Therefore, the metal was exchanged with Teflon. The Teflon was tested prior use and were removable without any difficulties at the trial.

Despite the poor selection of press plates, the alignment had improved significantly in the upper layer compared to previous test coils. As shown by Figure 4.6 compared with 4.2b and 4.2c.

A side effect of excluding pressure along the whole surface of the coil, was that the epoxy did not harden with a flat surface. The rough surface, caused by the combination of too much epoxy and the lack of pressure downwards while hardening does not represent any major issues, but is not desirable. However, the winding procedure takes too long for the hardening process of the epoxy not affect the epoxy feeder, and thereby, apply more epoxy than desired. The excess epoxy did influence the width of the circular section of the coil, as this section does not harden with pressure towards center as the straight section, hence the upper layer is wider than the lower along the circular section. The width difference is shown in Figure 4.6a and 4.6b. This outcome would be prevented by mixing the epoxy in two sections instead of one.

The variation amongst dimensions is not the major problem caused by the hardening of the epoxy. As the epoxy hardens, the pulling resistance increases and the movement of the epoxy epoxy feeder increases. The superconductor can only be allowed to bend in one direction without the risk of damaging the MgB_2 filaments. Ergo movement and twisting of the epoxy epoxy feeder must be prevented. Measures was taken, and a damper was implemented. During a trial the damper did not prevent any unwanted movement. It made the epoxy feeder loose its flexibility, thus increase the risk of damaging the superconductor. The issue was solved by increasing the distance from the pulling force stabilizers and thereby lower the movement as the angle is reduced.

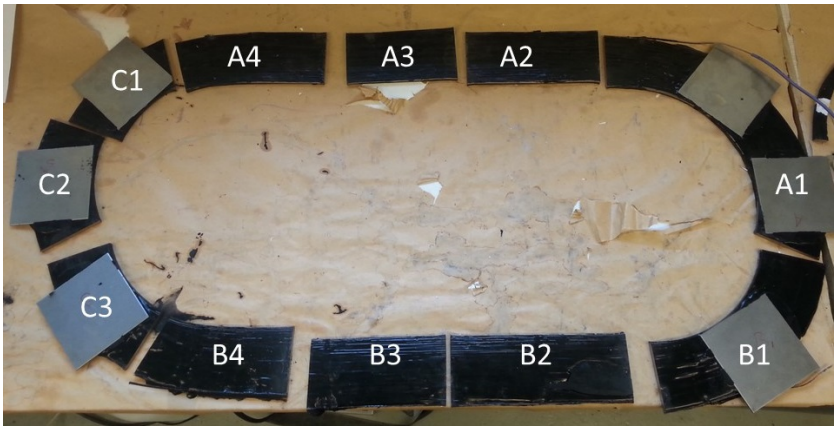

Figure 4.5: Cuts made to verify alignment of upper layer.

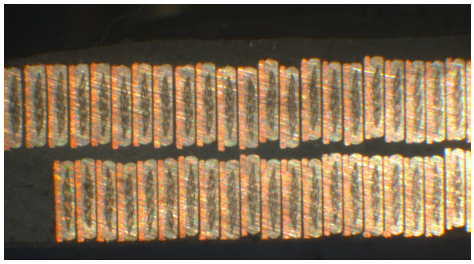

(a) B1 towards the outside.

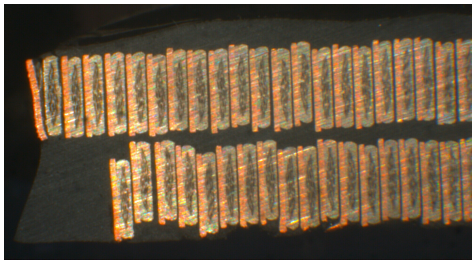

(b) C3 towards the outside.

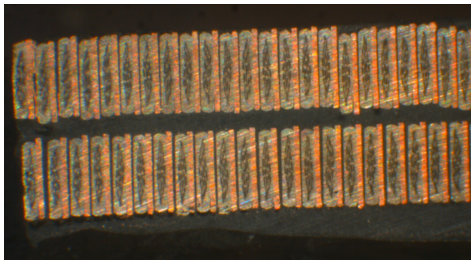

(c) C3 towards center.

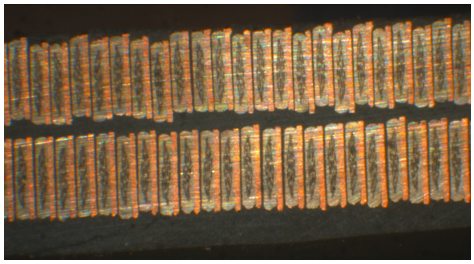

(d) C3 middle part.

Figure 4.6: Alignment of turns in upper and lower layer in the full scale test coil.

4.3 Impact of Turn-to-Turn Contacts

In pure DC operations, a superconducting coil would not have use for any insulating material at all, since the current would flow only and loss free in the superconducting filaments. Under such conditions, voltage between turns will not occur. However, during real operations this is not the case. Flux flow losses, as described in section 2.3.1, will give rise to a small DC turn-to-turn voltage. During ramping of the current, the voltage across the entire coil will be determined by $U_{coil} = L \cdot dI/dt$ and in a practical wind turbine generator rotor, AC magnetic field are present, causes an induced voltage in the rotor windings [9].
During flux flow losses the DC electric field is normally given by

$$E_{DC} = E_0(\frac{I}{I_C})^n \tag{4.2}$$

where E_0 is $1 \times 10^{-4}\,\mathrm{V\,m^{-1}}$, I is transport current in the superconductor, I_C is its in-field critical current, and n is an empirically determined exponent. For an MgB_2 wire operated at a safety margin of 25 % and a typical n value of 20, E becomes $0.3\,\mu\mathrm{V\,m^{-1}}$. For one turn in the large scale, full generator pole the voltage will be $2\,\mu\mathrm{V}$.

During current ramping the average voltage would become in order of magnitude of 5 mV when assumed that the inductance of the coil is somewhat around 10 H for the large scale full generator pole, the ramping rate is $0.1\,\mathrm{A\,s^{-1}}$ and the voltage is evenly distributed along the coil.

A rough estimated turn-to-turn voltage caused by AC harmonics present in the rotor windings can be determined by

$$E_{coil} = \frac{d\phi}{dt}, \tag{4.3}$$

where ϕ to the enclosed magnetic flux. With a total area of the field winding in the 10 MW design of $1\,\mathrm{m^2}$, the turn voltage becomes approximately 40 mV [9].

Thereby, the critical operating point is the voltage due to AC harmonics and with the lowest discovered contact of $1.56\,\Omega$, an estimated current of 25.64 mA. This current is less than the 0.1 % of the DC current acceptable from the AC point of view [9].

Chapter 5

Room Temperature Parameters

Introduction

In this chapter, methods to determine the room temperature parameters are described. The parameters of interest is the resistance and the inductance. Each coil section has been measured individually and then combined, forming the entire coil. Different equipments have been used and the results are compared in this section.

5.1 Inductance Theory

The inductance is the relation between how much flux a circuit produce for a given current and are determined by:

$$L = \frac{\phi}{i} \tag{5.1}$$

where L is the inductance, ϕ the magnetic flux and i the current passing through the circuit [10]. The inductance is dependant by material properties and geometric shape and for a solenoid, the magnetic field inside is given by

$$B = \mu_0 \frac{N}{l} i \tag{5.2}$$

where μ_0 is the permeability in vacuum, N number of turns and i the current. The flux is then $\phi = BA$, where A is the area. The total magnetic flux linked with N turns becomes $\mu_0 N^2 Ai/l$. By inserting $E = -Ldi/dt$ into $E = -d\phi/dt$ gives

$$L = \mu_0 N^2 \frac{A}{l} \tag{5.3}$$

thus the inductance is dependant by the material magnetic properties (μ) and the geometric design (A and l) [11].

When implemented into a circuit the inductance is classified as a reactance and are given by

$$X_L = j\omega L = 2\pi f L. \tag{5.4}$$

The reactance is frequency dependant and the value is ohm [Ω]. Ohms law for alternating current is $V = I \cdot Z$, where Z is the impedance and given by $Z = R + jX$. For high frequencies the $R \ll X_L$ and the resistance may be excluded leading to $V = I \cdot X_L$. Then the inductance is given by

$$L = \frac{V}{I \cdot j2\pi f}. \tag{5.5}$$

5.2 LAB Setup

To determine the room temperature parameters the coils has been connected as illustrated in Figure 5.1. The instruments used is listed in Table 5.1.

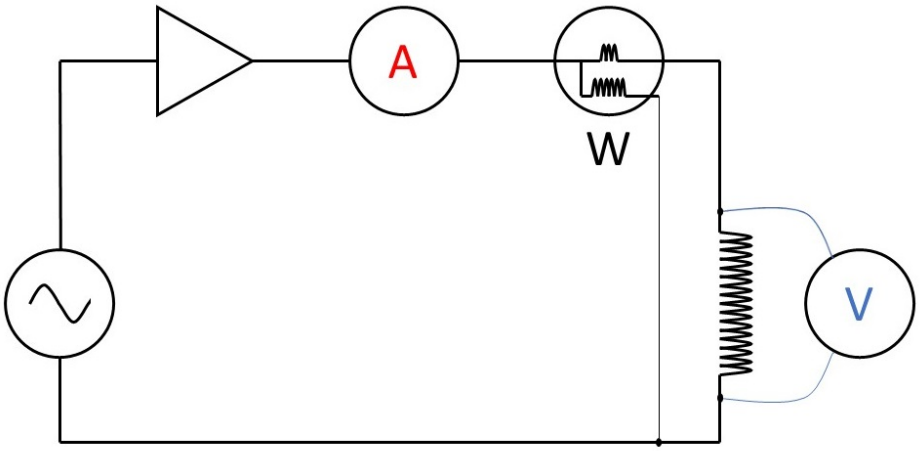

Figure 5.1: LAB setup

Table 5.1: Test equipment

Equipment	Producer
Signal generator	TECHSTAR (Kenwood)
Amplifier	Toellner
Ammeter	Keithley
Watt-meter	YOKOGAWA
Voltmeter	FLUKE
RCL-meter	AGILENT

The respective coil sections has been measured at three different frequencies and currents. The required measurements to calculate inductance is the current, voltage and frequency for high frequencies while at low frequencies the power and power factor is also needed. Due to susceptibility of the nickel, results is based on high frequencies (and excluding R) as hysteresis losses impact the measured power. Additionally a RCL-meter has been used to compare the results.

5.3 Results

The determination of room temperature parameters are given in Table 5.2. The measured values are given in Appendix E.

Table 5.2: Results of room temperature parameters of coil sections individually and combined.

Coil Section	$R_{DC}[\Omega]$	L[mH]	L_{RCL}[mH]
1	10.17	53.6580	54.00
2	9.94	54.0011	53.84
3	9.87	53.2268	53.19
4	9.92	54.3100	53.95
5	9.95	54.1464	53.98
6	9.97	53.9721	54.02
7	9.92	53.5487	53.25
8	9.90	53.1300	53.28
9	9.94	54.4714	53.52
10	9.88	54.4127	53.32
11	9.90	54.3621	53.75
1/2 coil (2-6)	49.69	1149.7721	-
1/1 Coil (2-11)	99,89	4490.3465	-

Chapter 6

Soldering Method and Soldering Tool

Introduction

The MgB_2 superconducting coil is constructed out of ten double pancake coils. In previous Master theses,[12] and [13] the joints were soldered. Different soldering techniques were discussed in Sindres Master thesis, and he departed with modified high power soldering iron.

Previous soldering tasks had been done on a MgB_2 wire with different structure, where the copper is embedded in the core of the nickel sheet. This differ from the wire which has been used in this project and soldering of joints may disrupt the existing soldering between the nickel sheet and the external copper stabilizer. This of course, is dependant on the choice of solder and its melting temperature. However, lead free solder is preferable due to avoidance of heavy metals, thus it has a significantly higher melting point and thereby increasing the risk of damaging the original soldering.

6.1 Soldering Tool

A high power soldering iron has been modified to solder the joints of the MgB_2 coil. The iron tip has been replaced by a custom made copper mold. This copper mold is designed to make a joint with low resistivity and without damaging the superconductor wire. In Figure 6.1 the bending radius while soldering is illustrated and, as shown, the bending radius does exceed the minimum bending radius of 75 mm. Thus, no degradation of critical current will occur as described in section 2.4.1.

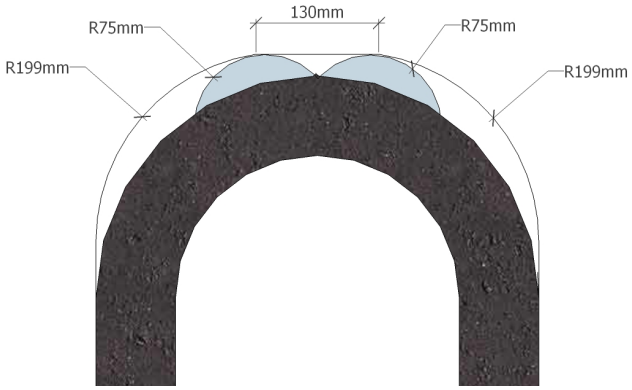

Figure 6.1: Bending radius while soldering.

As displayed in Figure 6.2, the mold is composed of a massive copper plate with brass screws and placement barriers. A second copper plate is threaded down the screws and attached with wingnuts and springs. These springs apply pressure while soldering so that the layer of solder is as thin as possible, hence the resistance of the joint is as low as possible. The screws is entered from beneath the copper mold because the brass screws tend to get stuck in the copper mold after heating due to different heat expansion. Otherwise, it would not be possible to remove the soldering tool after making a joint. A more detailed drawing of the soldering tool can be found in Appendix F.

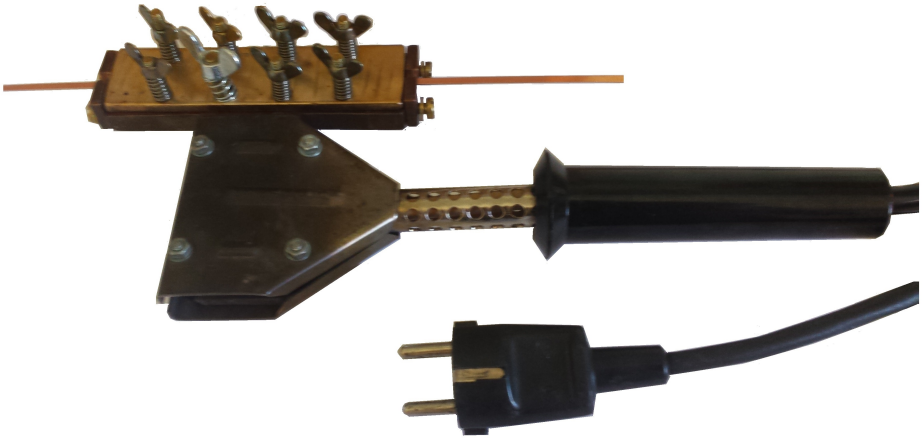

Figure 6.2: Soldering tool.

6.2 Making of Joints

The soldering process starts out with cleansing the surfaces which shall be soldered. This can be done with either acetone or Isopropanol. Then the surfaces are pre-soldered, a procedure that requires proper solder and flux agent.

It is difficult to attach solder onto nickel, and no low temperature solder had successfully been attached to the nickel sheet with the combination of flux agent Decaflux: Pincel Ecogel. However, lead-free solder (ISO-core Sn99.3/Cu0.7AgNiGe.) with a melting temperature of 227 °C and the use of ISO-flux EL3202A would attach easily. Nevertheless, due to higher soldering temperature, the MgB_2 wire could fracture in the soldering between the nickel and the external copper stabilizer, as shown in Figure 6.3. The pre-soldered nickel sheet and external copper stabilizer is placed onto each other and wrapped in aluminium foil to avoid attachment to the copper soldering tool.

The wrapped joint is then placed within the placement barriers, a thermocouple type K is placed on top of the joint before the second copper plate is attached and screws are tightened until the springs is almost pressed together. The soldering tool is connected to the 230 V grid and disconnected when the desired temperature is reached. Due to the high mass, the temperature will continue to rise a couple of °C (normally 1 - 5 °C). The soldering tool will then cool naturally before disassembly. The heat-profile can be found in Appendix G. A sample has been cut in half and studied under a microscope to determine the thickness of the solder between the wires. The thickness is estimated to 80 µm. The cross-section is displayed in Figure 6.5.

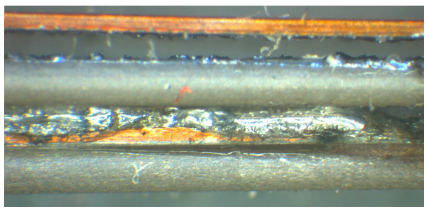

Figure 6.3: Illustration of fracture in the bonding of a MgB_2 wire.

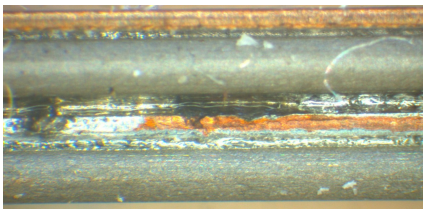

Figure 6.4: Illustration of a MgB_2 joint.

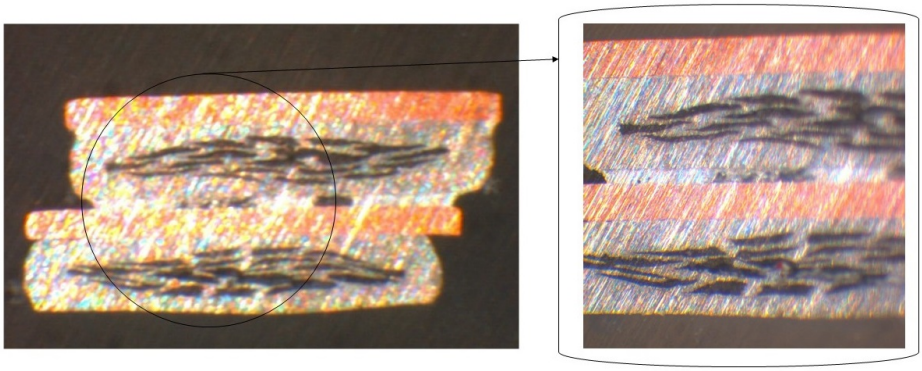

Figure 6.5: Soldered cross-section of MgB_2.

6.3 Testing of Joint

To ensure that the soldering tool makes sufficient joints, a joint has been made and the resistance has been measured. This test has been conducted on a DI-BSCCO (HTC) superconductor and not on the MgB_2 wire. The HTC is selected for this test due to the opportunity to perform measurement when in superconducting state, as this wire has a transition temperature above that of liquid nitrogen. The sample, shown in Figure 6.6 , was first pre-soldered with solder SR37 LFM-48 S produced by Almit. Then the two pre-soldered surfaces was placed onto another and placed into the soldering tool. To avoid that the soldering shall attach to the copper of the soldering tool, the joint is wrapped in aluminium foil. The soldering tool is then heated up to 230 °C and shut of. The device is cooled naturally, before disassembly and the joint is removed. The estimated thickness of the soldering is 12 µm.

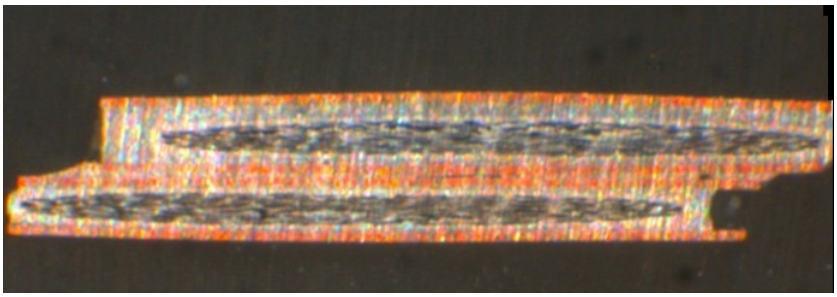

Figure 6.6: Illustration of a copper alloy laminated BSCCO joint.

To determine the resistivity of the joint the four-probe technique has been

used. Under room temperature conditions the joint has a resistance of 2.24 Ω. When submerged in liquid nitrogen, the measurements became unstable and did not act linear with the current. As the current was shut off, the voltage would rise and fall on its own. This may originate from the high temperature difference along the measuring probes, thus act as a thermocouple. The voltage would rise or fall when the measuring probes where submerged further into the liquid helium, which supports the assumption of a thermocouple affect. When the voltage was somewhat stable, a current of 15 - 45 A was injected through the joint, and the voltage would rise approximately 1 - 2 µV. Thus, the attempt to find the joint resistance was inconclusive and not linear as it should have been. However, this indicates that the resistivity of the joint is below 50 nΩ and will produce an effect of 1 - 5 mW.

Chapter 7

Discussion

In this master thesis, the possibility of constructing a generator pole without specific turn-to-turn insulation has been examined. The wet winding technique may be a viable and attractive method to reduce costs, as electrical insulation, like Kapton, represent approximately 10 % of the MgB_2 superconducting wire costs. In addition, by excluding the insulation, the coil will be densified by about 10 %. A denser coil will increase thermal and electrical stabilities as discovered by OJ Kwon et al in [14]. In addition, the overall current density will be increased.

In pure DC operations, a superconducting coil would not have use for any insulating material at all, since the current would flow only and loss free in the superconducting filaments. However, during ramping of current, it would give rise in the turn-to-turn voltage due to the change in the enclosed flux inside the coil. This represent a critical operating state of non-insulated coil and therefore, a slow ramping rate of the current is required to avoid current to flow between turns and dissipate heat as reported by Heecheol Park et al in [15].

For this project a MgB_2 superconductor has been chosen and wound into a double pancake coil. Due to its relative high operating temperature of 15 - 20 K it is possible to operate without the use of hazardous liquid nitrogen. It has relative low cost compared to HTC cuprates and can be produce in long lengths with the power in tube technique. Ideal for magnet application. However, the reliability needs to be proven.

In comparison, other superconductor like NbTi, widely used in MRI machines, which are available for one tenth of the price of the MgB_2 wire at today's prices, classified by euros per kA m. The NbTi can produce a higher

magnetic field and conduct a larger current. However, operating temperature at 4.2 K is a major downside, as cooling system will be costly. YBCO, which has similar properties of the MgB_2 except from operating temperature and price. Operating temperature will be at the range of 40 - 50 K, and the price is approximately thirty times higher than MgB_2. However, both the YBCO and the MgB_2 has the advantage of future cost reduction due to large-scale deployment. Nevertheless, the MgB_2 conductors are still under development and future enhancements will be expected. This makes the MgB_2 a good choice to reduce cost, which will be further reduced if wound without specific turn-to-turn insulation.

The soldering tool developed during this project was intended to make a joint with low resistivity and without damaging the superconductor. Due to the fabrication method of the MgB_2, the choice of solder and its melting temperature is a decisive factor. As the cladding material and external copper stabilizer is soldered together, if the chosen melting temperature is to high, the result will be fractures in the existing bonding. However, the consequence of these fractures will not impact the filaments but it may reduce thermal stability in an area that will produce heat, which need to be transported away form the joint. It is possible that the situation is easily solved with clamps along the conductor close to the soldering tool to maintain the bonding while soldering. However, the appliance of solder under the pre-soldering share the same risk with respect to fractures in the bonding. In addition, during this stage the superconductor can be easily damaged due to unwanted movement. Unfortunately, no low temperature solder would attached to the nickel sheet. Nevertheless, it has been achieved with solder containing lead by Sindre Sætre[12] and Eivind Engebrethsen[13]. It is possible use same solder and flux agent as lead based solder has lower melting point than lead-free. This was refused to be supplied by the NTNU service lab, due to involvement of heavy metals. Therefore this combination of solder and flux agent has not been testet. The soldering tool is made out of copper. This is chosen due to excellent thermal conductivity, unfortunately the joint will attach to the copper mold due to excess solder which is pressed out on the sides of the joint when melted. This is solved by wrapping the joint in alumina foil during soldering, which could have been avoided by constructing the mold in aluminium.

A joint has been made with YBCO-superconductors and tested when submerged in liquid nitrogen. This superconductor was chosen due to the advantage of the opportunity to test while in superconducting state. It is assumed that the joint resistance would be slightly lower for this supercon-

ductor due to the lower cross-section, and the distance to the superconducting filaments are shorter than for an MgB_2 wire. Nevertheless, it is assumed that the magnitude would be in somewhat the same region. The test results where to some extent inconclusive, as the resistance for a 10 cm joint is difficult to measure. This was also experienced by Sindre Sætre [12]. However, his results was 37 and 48 nΩ, while the estimate in this thesis is approximately 50 nΩ.

The insulating ability of the epoxy has been tested by an ohm-meter, and values below one Ω has been determined by the more precise four-probe technique. Due to the size of the MgB_2, this task require a microscope. When performing such measurements on very small surfaces, the probes may be problematic to place in contact with the respective turns. In that matter, the OL (overload) results will not be reliable due to the possibility that measuring probes do not have contact with the superconductor. This occurred often, and results that indicated high contact resistance where more reliable than those of OL. Nevertheless, as a procedure, the probe contact was confirmed by placing both probes on the same turn, before moving one probe to the neighbor turn. If the result where OL, the second probe was also moved to the neighbor turn to confirm contact between probes and test object at both turns. The winding method showed no low value (<1 Ω) in the test coils made except from one single contact. Closer study revealed that a silver tip had penetrated the epoxy and made contact with its neighbor turn. Thus contamination or imperfection of fabrication was the reason for the contact, and not a result of poor appliance of epoxy.

Chapter 8

Conclusion

This study is a part of research in the forefront, investigating the possibility to implement superconducting magnet technology in a multi-pole generator for future large offshore wind power, to drive down the cost of wind energy. During the project period, it has been produced and tested a small scale and a full scale double pancake coils with respect to insulating ability of epoxy. A soldering technique has been developed and tested, with a modified high power soldering iron. Furthermore, a full generator pole has been constructed and room temperature parameters has been determined.

The insulating ability of epoxy has been determined, and results indicate that no low resistive contacts between turns will occur. This leading to the conclusion that the coil may be safely operated during normal DC condition, DC ramping and AC harmonics. Where maximum leakage current would be approximately 25 mA. This current is less than the 0.1 % of the DC current acceptable from the AC point of view. However, one occasion of internal contact was discovered, assumed to originate from fabrication. This implies that a better control of conductor dimensions is needed to ensure that low resistance contacts in the order below 1 Ω will not occur.

To connect the ten double pancake coils constructed during this master thesis, a soldering technique has been developed and tested. The resistivity has been determined to be in the region of 50 nΩ which will produce an effect of 3.125 mW at operating current of 250 A. However, further testing with low temperature solder is necessary to exclude the risk of fracture in existing bonding of MgB_2 wire.

The room temperature parameters has been determined by energizing the coil with DC & AC currents, leading to a resistance of 99.89 Ω and induc-

tance of 4.49 H.

Chapter 9

Recommendation for Further Work

Followed are tasks that should be considered in further work:

Removal of excess epoxy
While the coils hardened, excess epoxy floated out along the sides. On the coils, where press plates have been used, the surface is rough and should be even out. Thus, the excess epoxy should be sanded to achieve as dense a coil as possible.

Casting the coil sections together
The ten coils should be cast together onto the thermal interface to achieve a best possible thermal conductivity.

Solder the connection between coil sections
The coil sections need to be connected. This can be done by the soldering procedure developed in chapter 6. However, the consequences of fractures of the bond between the nickel sheet and external copper stabilizer must be either evaluated or excluded.

Provide mechanical support
The coil will not be able to absorb the Lorentz-forces which act on the coil when operated at rated current. Therefore, mechanical support needs to be calculated and addressed accordingly.

Investigate the act of thermal reduction
As temperature decreases the various substances will contract differently. To maintain maximum thermal conductivity it is important to investigate the consequences of this thermal reduction.

Test the coil under superconducting conditions.
To validate the coil, and investigate that it will be able to produce the desired magnetic field, the coil need to be refrigerated to rated temperature and energized. In order to do so, a test program should be designed. This test program should include the determination of a current source, which ought to provide a stable current with low ramping rate to a basically pure inductive circuit. To ensure the safety of the coil, the test setup needs to be implemented with a quench protection. In addition, a measurement system for voltages, temperatures, etc. is desirable.

Bibliography

[1] A B Abrahamsen, N Mijatovic, E Seiler, T Zirngibl, C Traaeholt, P B Norgaard, N F Pedersen, N H Andersen, and J Ostergaard. Superconducting wind turbine generators. *Superconductor Science and Technology*, 23(3):034019, 2010.

[2] Arthouros Zervos and Christian Kjaer. Pure power wind energy targets for 2020 and 2030. Technical report, European Wind Energy Association, November 2009.

[3] N. Magnusson, B. B. Jensen, A. B. Abrahamsen, and A. Nysveen. Superconducting generator technology for large offshore wind turbines. Presentation SINTEF Energy Research.

[4] A. B. Abrahams, N. Mijatovic., E. Seiler, M. P. Sorensen, M. Koch, P. B. Norgaard, N. F. Pedersen, C. Traeholt, N. H. Andersen, and J. Ostergaard. Design study of 10 kw superconducting generator for wind turbine applications. *IEEE TRANSACTIONS ON APPLIED SUPERCONDUCTIVITY*, 19(3):1678–1682, June 2009.

[5] G. Snitchler, B. Gamble, C. King, and P. Winn. 10 mw class superconductor wind turbine generators. *Applied Superconductivity, IEEE Transactions on*, 21(3):1089–1092, June 2011.

[6] R.G Sharma. *Superconductivity : Basics and Applications to MagnetSuperconductivity : Basics and Applications to Magnets*, volume 1. Springer International Publishing, 2015.

[7] Jun Nagamatsu, Norimasa Nakagawa, Takahiro Muranaka, Yuji Zenitani, and Jun and Akimitsu. Superconductivity at 39[thinsp]k in magnesium diboride. *Nature*, 410(6824):63–64, 2001.

[8] Jan Christian Eliassen. Methods for winding uninsulated superconductor ccoil with mgb2. Technical report, Norwegian University of Science and Technology, 2015.

[9] N. Magnusson et al. Design aspects on winding of an mgb2 superconducting generatge coil. *SciVerse ScienceDirect*, 2015.

[10] Robert Nilssen. *Electromagnetics in Power Engineering*. NTNU, 2012.

[11] D. C Tayal. *Electricity and magnetism*. Himalaya Publishing House, 2009.

[12] Frode Sætre. Splicing and coil winding of mgb2 superconductors. Master's thesis, Norwegian University of Science and Technology, Department of Electrical Power Engineering, 2008.

[13] Eivind Engebrethsen. Testing av superledende spoler, 2009.

[14] OJ Kwon et al. Effects of turn-to-turn compactness in the straight sections of hts racetrack coils on thermal and electrical characteristics. *Superconductor Science and Technology*, 26(8), 2013.

[15] Heecheol Park, A rong Kim, Seokho Kim, Minwon Park, Kwangmin Kim, and Taejun Park. Mechanical and electric characteristics of vacuum impregnated no-insulation hts coil. *Physica C: Superconductivity*, 504(0):138–143, 2014.

Appendix A

Moveable Rack Design

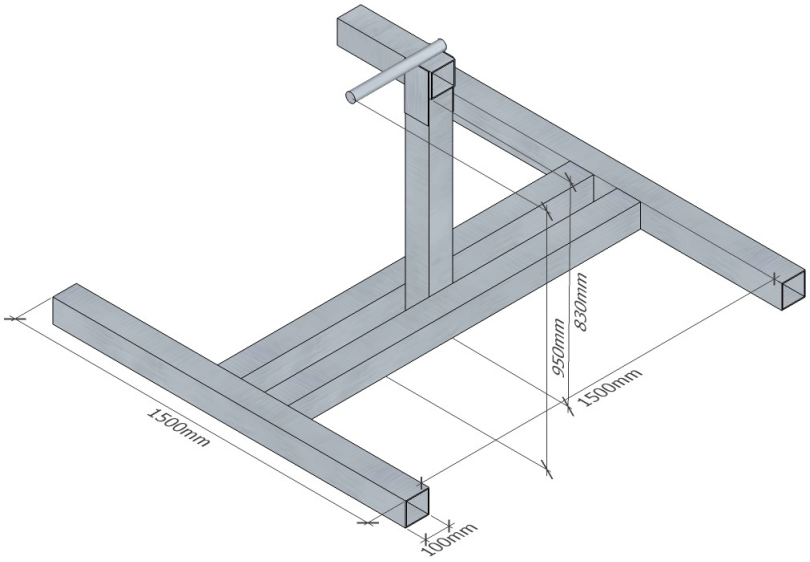

Appendix B

Winding Table Dimensions

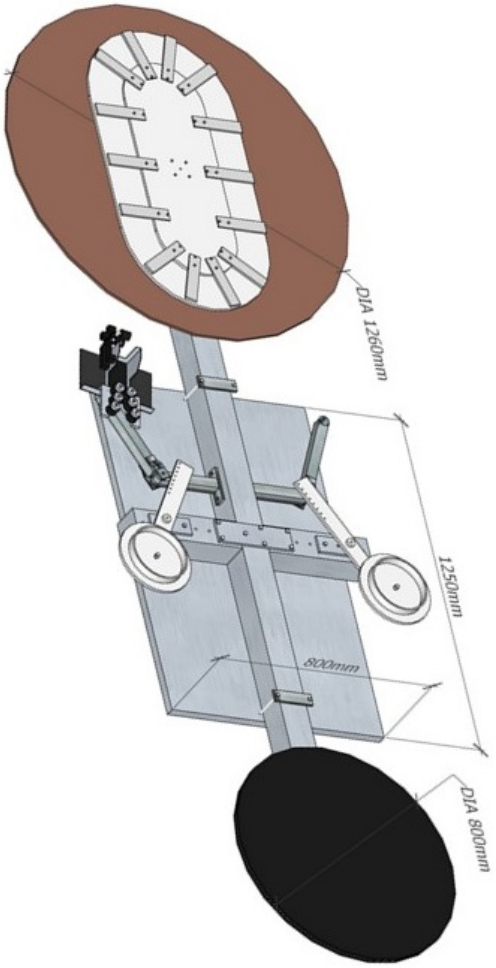

B.1 Mold Dimensions

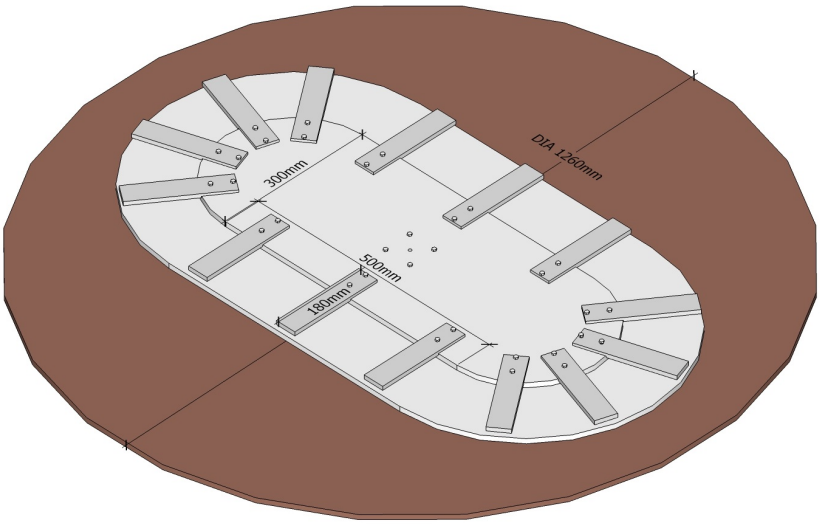

B.2 Pulling Force Stabilizer

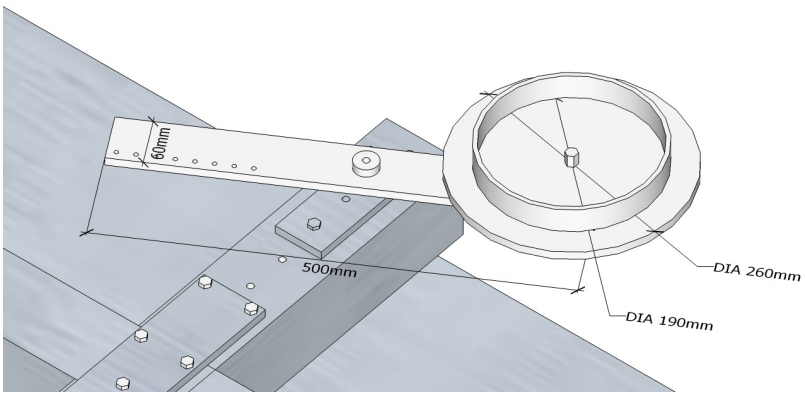

B.3 Epoxy Feeder

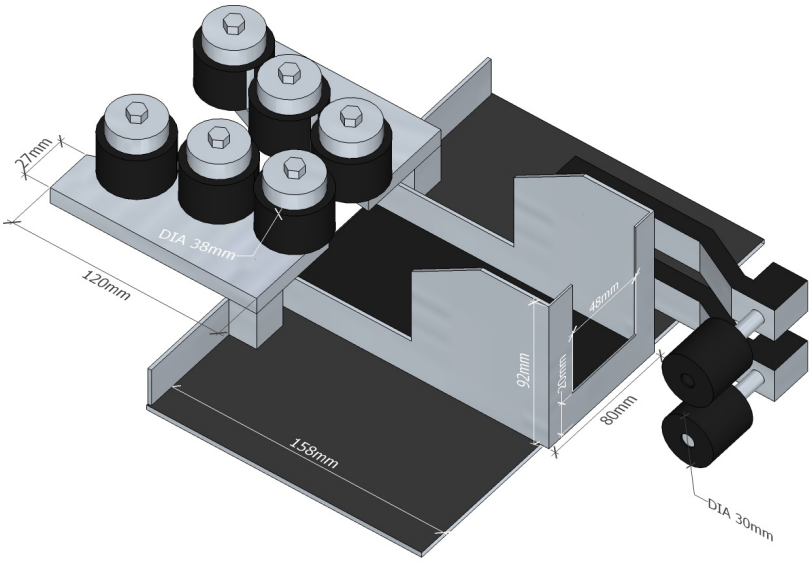

B.4 Epoxy Container

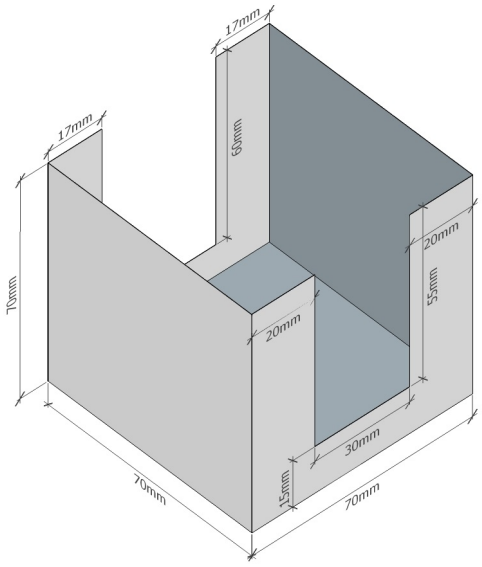

B.5 Press Plate

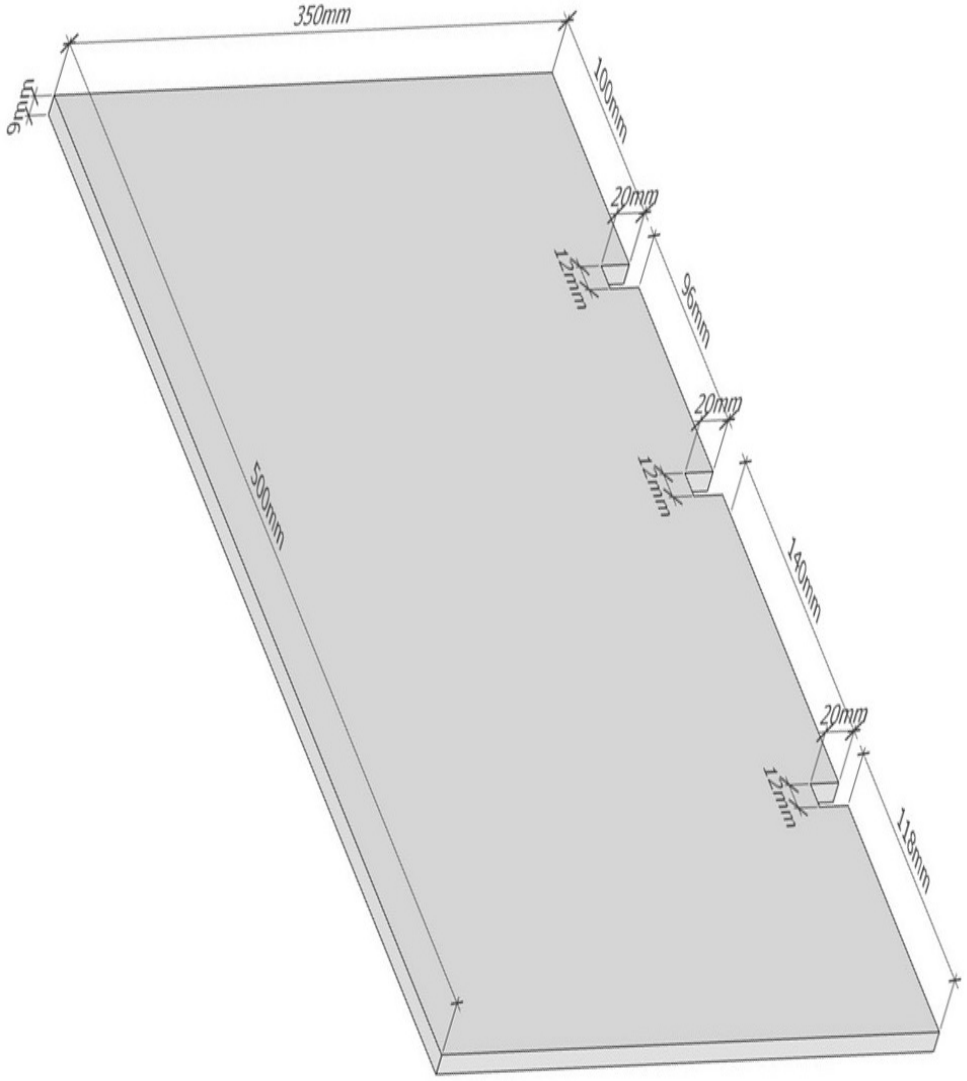

Appendix C

Results of Resistance Measurement Small Scale Winding

In this appendix the insulation test results is presented. The resistance value is given in Ω. Every turn-to-turn resistance is presented.

C.1 Upper Layer Test Object One

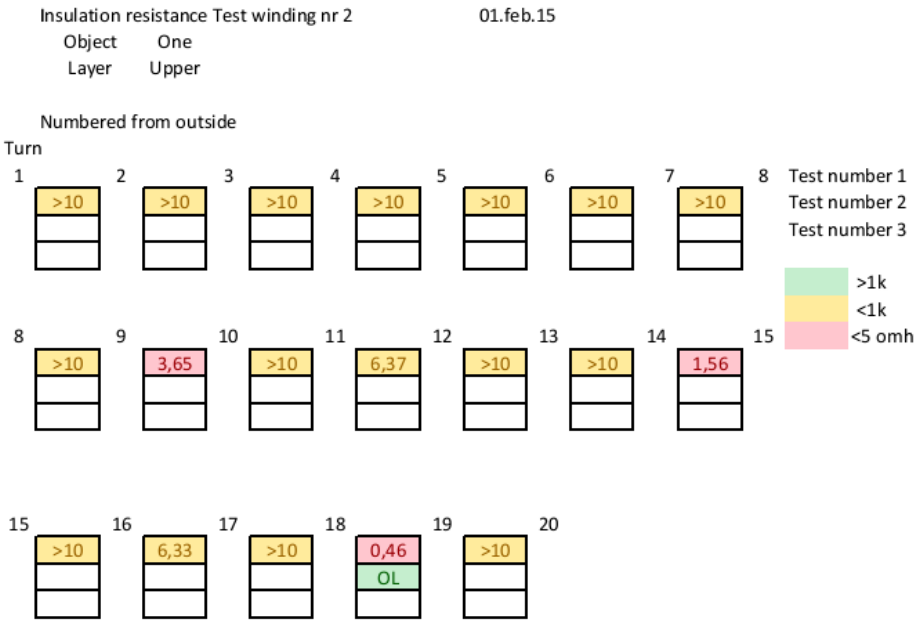

C.2 Lower Layer Test Object One

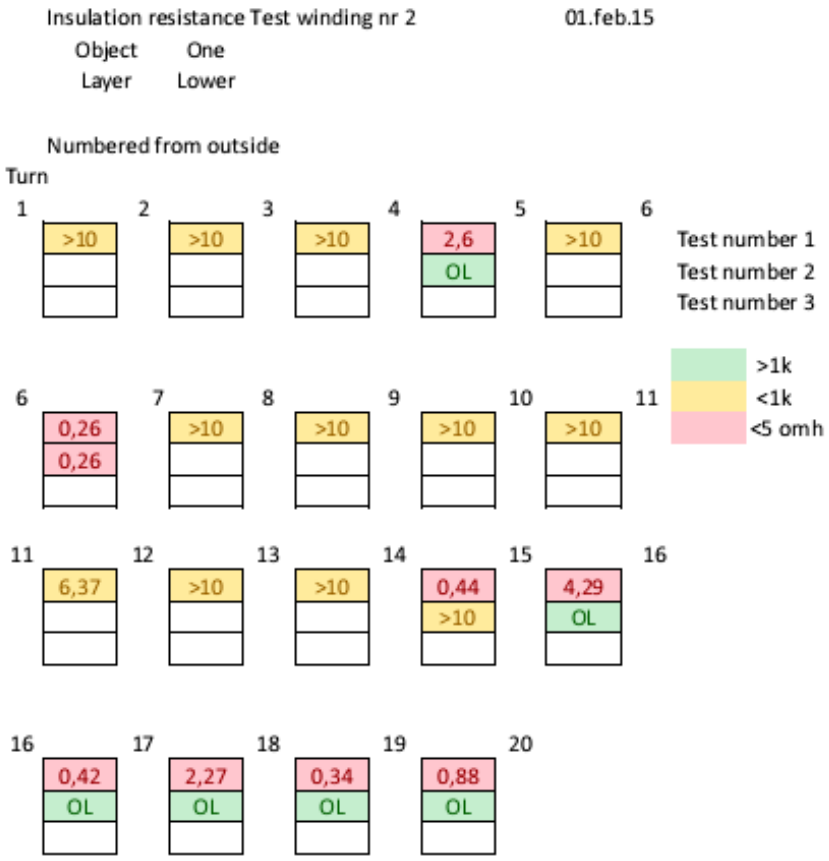

C.3 Upper Layer Test Object Two

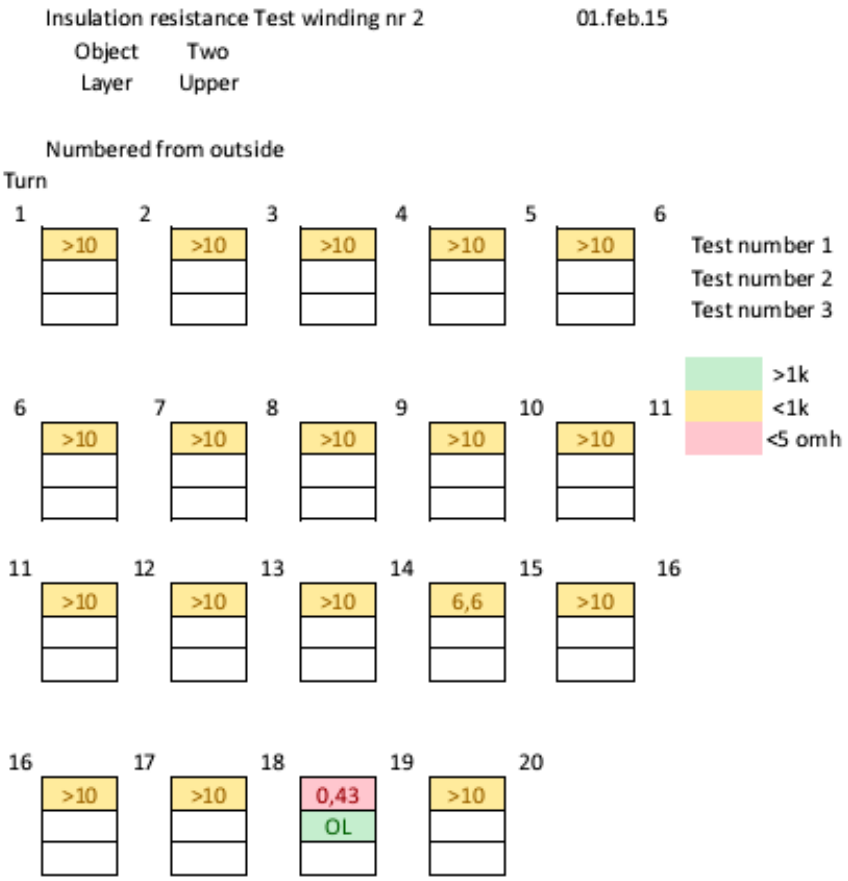

C.4 Lower Layer Test Object Two

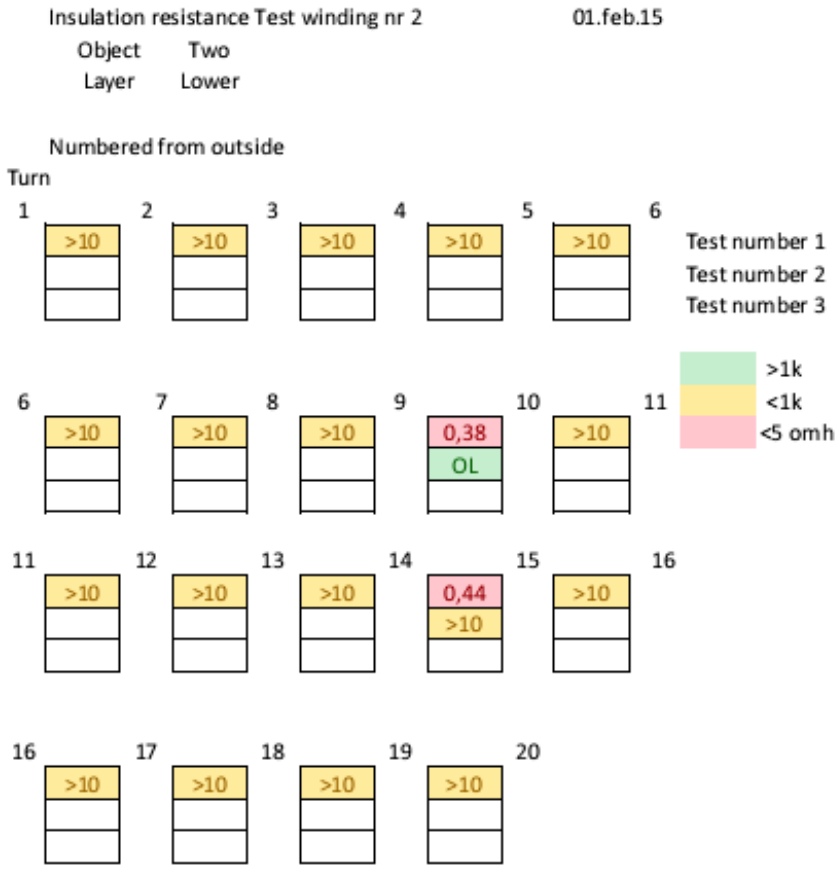

Appendix D

Results of Resistance Measurement Full Scale Test Winding

In this appendix the insulation test results is presented. The resistance value is given in Ω. Only the noteworthy turn-to-turn resistance is presented. The excluded values are in the range of 1 kΩ - ∞

D.1 Upper Layer Test Object A

D.2 Lower Layer Test Object A

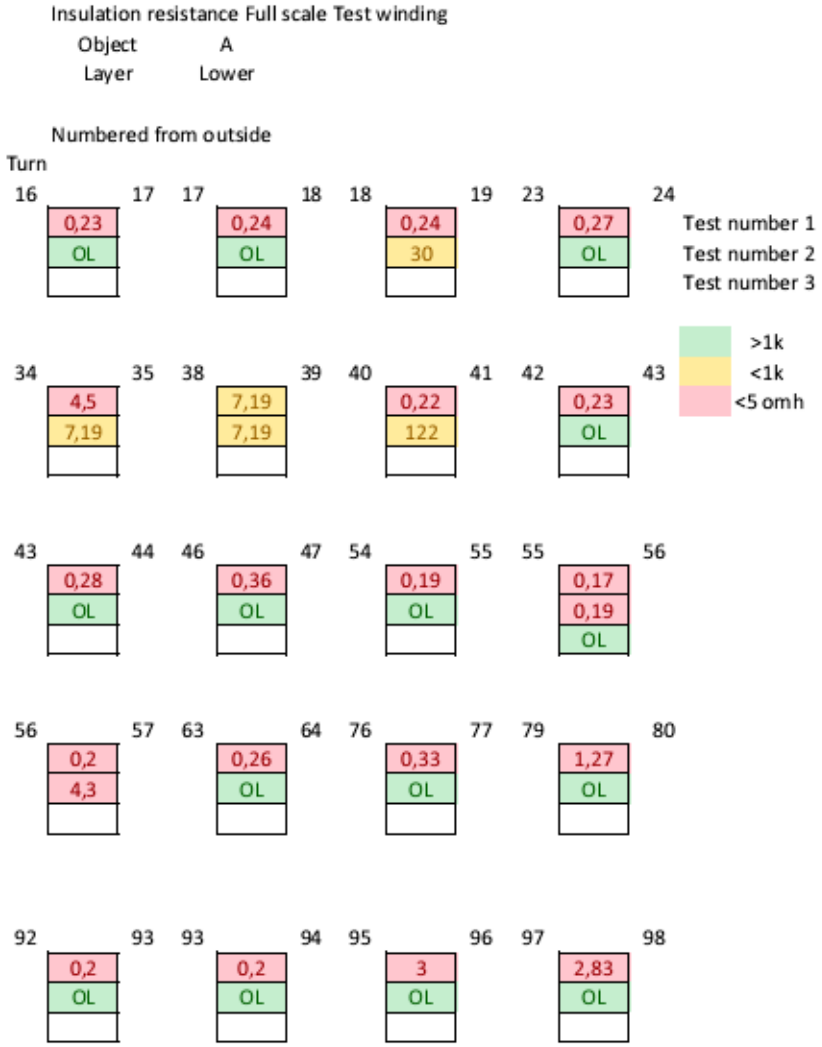

D.3 Upper Layer Test Object B

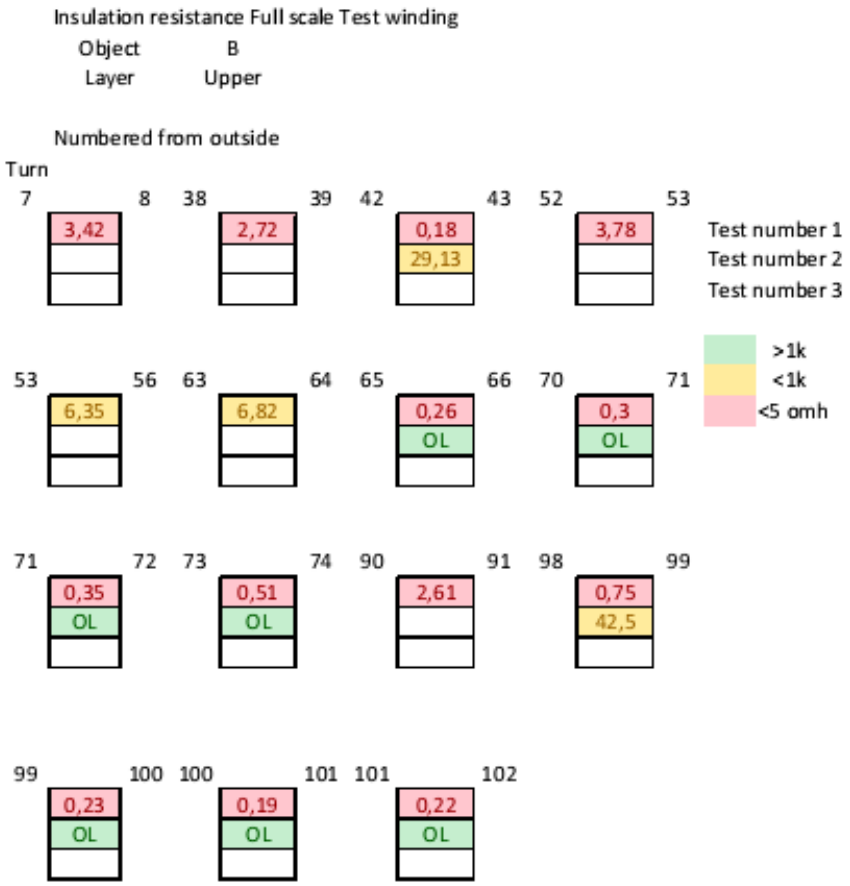

D.4 Lower Layer Test Object B

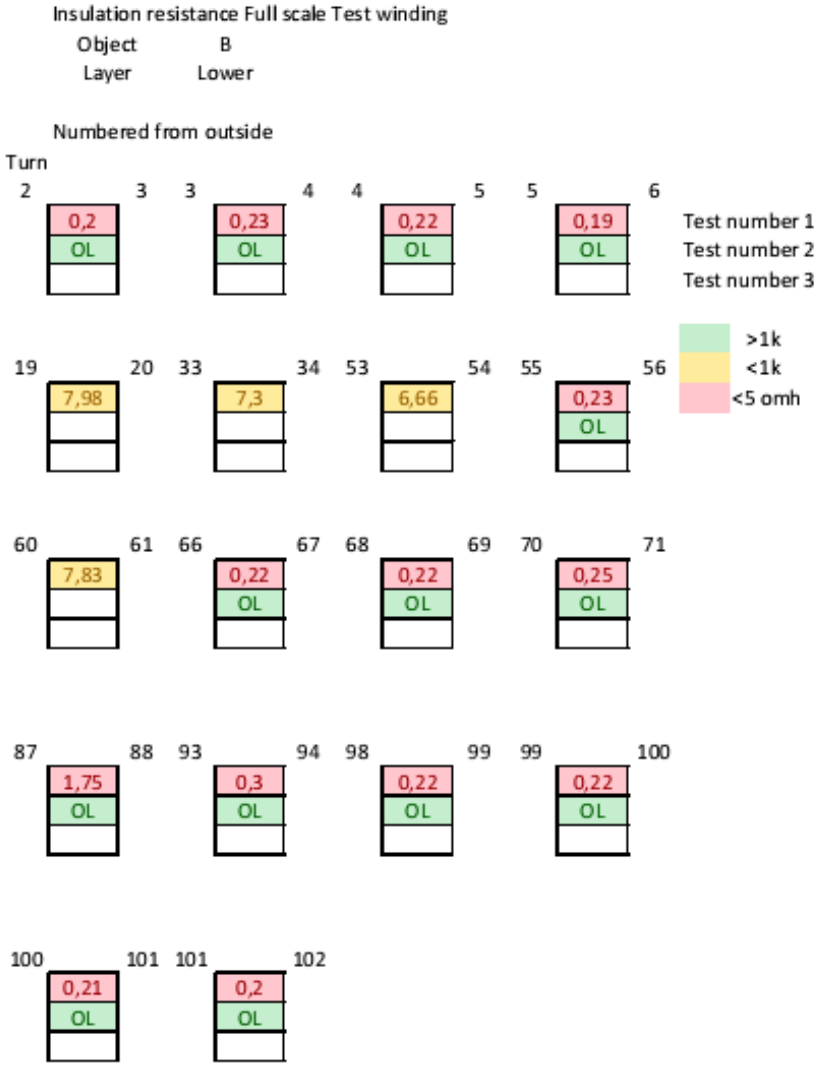

D.5 Upper Layer Test Object C

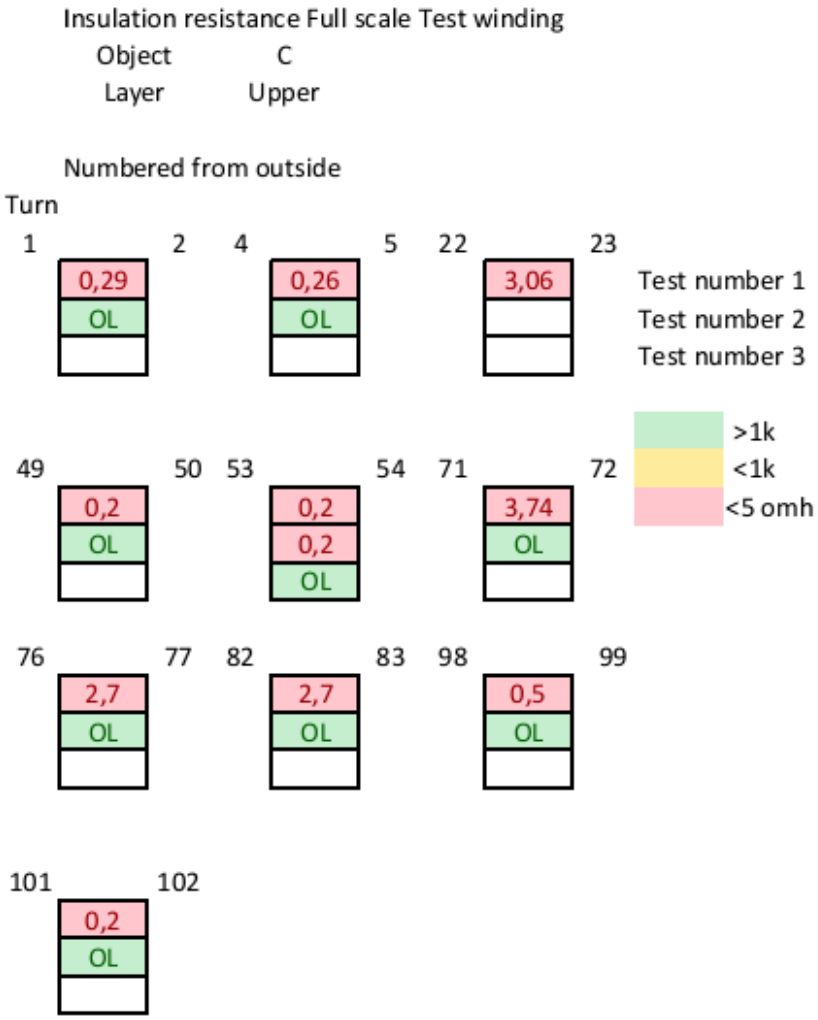

D.6 Lower Layer Test Object C

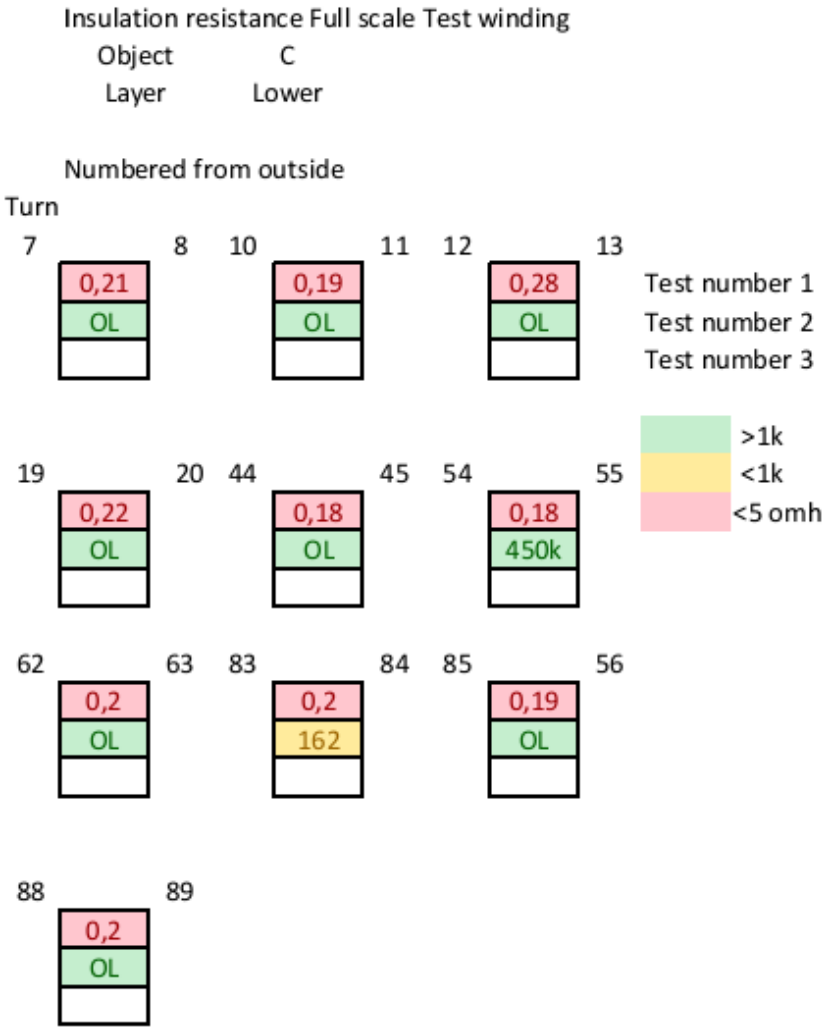

Appendix E

Room Temperature Parameters

E.1 Measurement Results

Coil Section	Frequency range	Fluke		Keithley	Wattmeter					
		V	f	A	V	A	P	Var	VA	PF
1	20Hz	2,03040	19,98700	0,15984	2,04000	0,16020	0,27000	0,18500	0,32700	0,82400
		5,94900	19,98700	0,46658	5,98000	0,46730	2,29200	1,59900	2,79500	0,82000
		0,60890	19,98900	0,04809	0,61000	0,04820	0,02500	0,01500	0,03000	0,86100
	220Hz	5,31600	221,26000	0,07061	5,32000	0,07070	0,07600	0,36900	0,37600	0,20300
		10,55100	221,26000	0,13944	10,56000	0,13960	0,29500	1,44400	1,47400	0,20000
2	20Hz	0,60500	19,98800	0,04835	0,61000	0,04850	0,02500	0,01500	0,03000	0,86100
		3,28820	19,98800	0,26147	3,31000	0,26200	0,70700	0,50200	0,86700	0,81600
		2,69660	19,98800	0,21435	2,71000	0,21470	0,47600	0,33500	0,58200	0,81600
	220Hz	10,11300	221,27000	0,13304	10,13000	0,13310	0,34900	1,30300	1,34900	0,25900
		5,16820	221,28000	0,06824	5,18000	0,06830	0,09300	0,34100	0,35400	0,26300
3	20Hz	2,01270	19,99300	0,16185	2,03000	0,16220	0,26900	0,18900	0,32900	0,81900
		7,45100	19,99200	0,59645	7,48000	0,59930	3,65100	2,59300	4,48000	0,81600
	220Hz	7,54300	221,27000	0,10154	7,65000	0,10160	0,20200	0,74100	0,76800	0,26400
		14,52700	221,28000	0,19458	14,55000	0,19460	0,74200	2,73000	2,82900	0,26200
		0,65040	221,28000	0,00880	0,65000	0,00900	0,00200	0,00500	0,00600	0,38500
4	20Hz	1,49050	19,99400	0,11888	1,50000	0,11920	0,14600	0,10300	0,17900	0,81700
		6,36700	19,99200	0,50549	6,40000	0,50630	2,63300	1,88600	3,23600	0,81300
	220Hz	7,47400	221,24000	0,09857	7,49000	0,09870	0,18200	0,71600	0,73900	0,24700
		13,75100	221,24000	0,18059	13,77000	0,18060	0,61100	2,41100	2,48700	0,24600
		0,64860	221,26000	0,00858	0,65000	0,00880	0,00300	0,00500	0,00600	0,39500
5	20Hz	0,59890	19,99300	0,04788	0,61000	0,04800	0,02500	0,01500	0,02900	0,85300
		1,42900	19,99200	0,11388	1,44000	0,11420	0,13500	0,09400	0,16400	0,82100
		4,19620	19,99300	0,33333	4,22000	0,33390	1,14800	0,81600	1,40900	0,81500
	220Hz	0,64440	221,24000	0,00851	0,06500	0,00870	0,00200	0,00500	0,00600	0,39900
		7,76200	221,24000	0,10224	7,77000	0,10230	0,20500	0,76900	0,79600	0,25700

Coil Section	Frequency range	Fluke		Keithley	Wattmeter					
		V	f	A	V	A	P	Var	VA	PF
6	20Hz	5,20490	19,99500	0,41288	5,24000	0,41360	1,76400	1,25800	2,16700	0,81400
		1,23910	19,99800	0,09866	1,25000	0,09890	0,10200	0,07000	0,12300	0,82600
		2,91770	19,99700	0,23174	2,94000	0,23220	0,55600	0,39500	0,68200	0,81500
	220Hz	0,64580	221,25000	0,00855	0,64000	0,00880	0,00200	0,00500	0,00600	0,39800
		7,62200	221,24000	0,10071	7,63000	0,10080	0,19300	0,74500	0,76900	0,25100
7	20Hz	0,59390	20,00000	0,04765	0,60000	0,04780	0,02400	0,01600	0,02900	0,83900
		1,29330	19,99900	0,10357	1,30000	0,10390	0,11100	0,07800	0,13500	0,82500
		4,04820	19,99800	0,32296	4,07000	0,32380	1,07500	0,76200	1,31900	0,81600
	220Hz	0,64290	221,22000	0,00860	0,65000	0,00880	0,00200	0,00500	0,00600	0,39700
		8,11300	221,22000	0,10804	8,13000	0,10810	0,23600	0,84700	0,88000	0,26900
		12,17600	221,23000	0,16175	12,21000	0,16180	0,52900	1,90300	1,97500	0,26800
8	20Hz	0,59220	20,00300	0,04764	0,60000	0,04780	0,02300	0,01700	0,02900	0,84000
		1,93600	20,00300	0,15510	1,95000	0,15550	0,24700	0,17400	0,30300	0,81700
		3,57990	20,00100	0,28626	3,60000	0,28690	0,84300	0,59700	1,03400	0,81600
	220Hz	0,64170	221,22000	0,00854	0,64000	0,00870	0,00200	0,00500	0,00600	0,40200
		1,33240	221,23000	0,01788	1,34000	0,01790	0,00700	0,02300	0,02400	0,31400
		5,88500	221,21000	0,07824	5,90000	0,07830	0,13600	0,44100	0,46200	0,29400
9	20Hz	1,65780	19,99200	0,13198	1,67000	0,13230	0,18100	0,12700	0,22100	0,81800
		4,91420	20,00800	0,39592	5,02000	0,39670	1,62400	1,15400	1,99100	0,81600
		10,16300	19,98900	0,80360	10,22000	-	6,69300			
	220Hz	0,63830	221,17000	0,00845	0.64	0,00860	0,00100			
		2,29060	221,18000	0,03000	2,30000	0,03040	0,01900			
10	20Hz	1,62440	19,99700	0,12996	1,63000	0,13030	0,17400	0,12300	0,21300	0,81700
		3,93150	19,99700	0,31372	3,95000	0,31440	1,00900	0,72500	1,24200	0,81200
		7,49500	19,99500	0,59617	7,53000	0,59720	3,64800	2,63100	4,49900	0,81100
	220Hz	5,24410	220,48000	0,06928	5,25000	0,06930	0,09100	0,35300	0,36400	0,25100
		10,54800	220,49000	0,13873	10,56000	0,13890	0,36700	1,42000	1,46600	0,25000
		14,23500	220,48000	0,18695	14,26000	0,18700	0,66600	2,58200	2,66500	0,25000

Appendix F

Soldering Tool

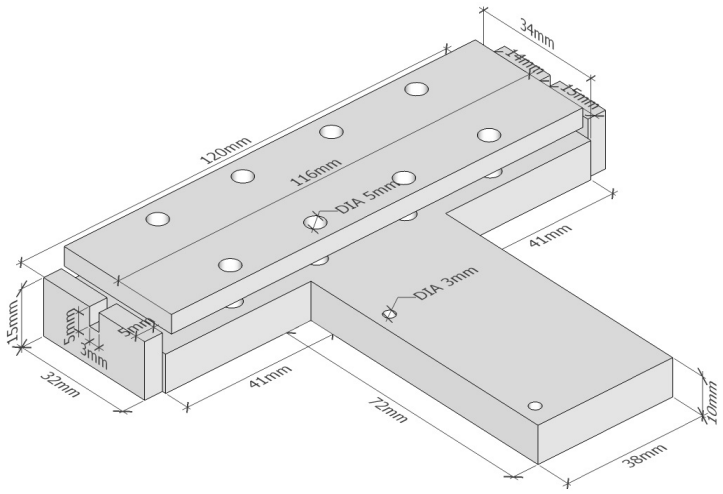

Appendix G

Heat Profile

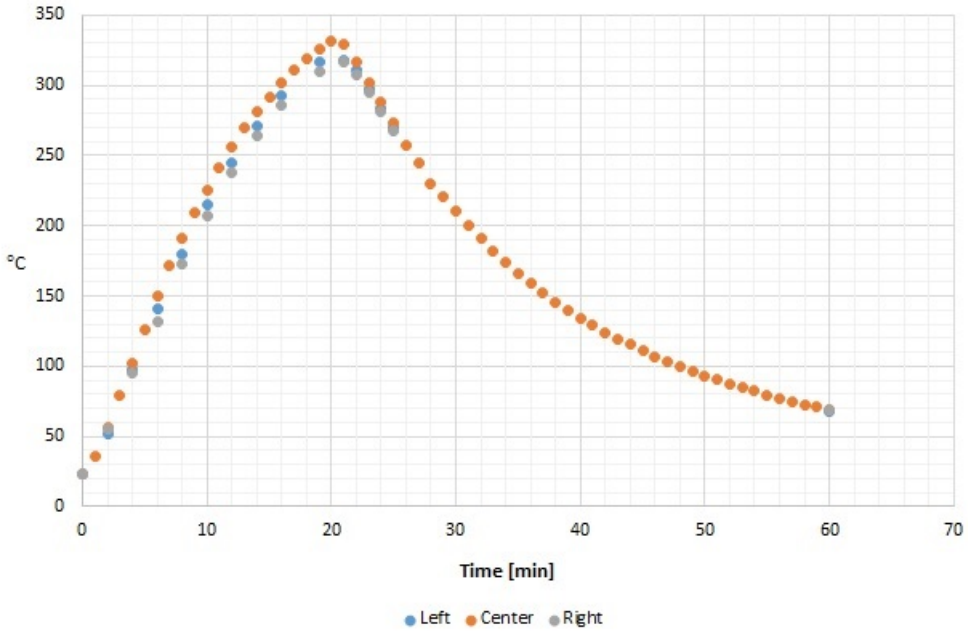

Appendix H

Published Paper

N. Magnusson, J. C. Eliassen,
A.B. Abrahamsen, A. Nysveen and P. King
Design aspects on winding of an MgB_2
superconducting generator coil
12th Deep Sea Offshore Wind R&D Conference, EERA DeepWind'2015

Available online at www.sciencedirect.com

SciVerse ScienceDirect

Energy Procedia 00 (2015) 000–000

Energy Procedia

www.elsevier.com/locate/procedia

12th Deep Sea Offshore Wind R&D Conference, EERA DeepWind'2015

Design aspects on winding of an MgB_2 superconducting generator coil

N. Magnusson[a,]*, J.C. Eliassen[b], A.B. Abrahamsen[c], A. Nysveen[b], J. Bjerkli[a], M. Runde[a] and P. King[a]

[a]*SINTEF Energy Research, Trondheim, Norway*
[b]*Norwegian University of Science and Technology, Department of Electric Power Engineering, Trondheim, Norway*
[c]*Technical University of Denmark, Department of Wind Energy, Roskilde, Denmark*

Abstract

Generators based on superconducting rotor coils are considered for future large off-shore wind turbines for their low weight and compact design, and for their possibility to reduce costs. In the 10-20 K temperature range, MgB_2 superconductors carry current densities 100 times higher than standard copper conductors at room temperature at one tenth of the wire cost per unit carried current. In the framework of the European project INNWIND.EU, an MgB_2 superconducting generator pole will be designed, built and tested. Some of the design aspects of this work with emphasis on the winding process and associated coil insulation are discussed. An overall high current density in the coil is of crucial importance to obtain clear benefits compared to conventional solutions. The wire itself may be the most important parameter in that respect. However, the overall current density of the coil is also influenced by the thickness of the turn-to-turn electrical insulation. Here we discuss the impact of the insulation and suggest the use of a one-step winding process, employing wet-winding, where the applied epoxy also constitutes the insulation layer between turns. In this way the coil is densified by approximately 10% compared to the use of an additional, dedicated, electrical insulation like Kapton for wet-winding or glass-fibre for dry-winding followed by vacuum impregnation. We show the results of a trial winding of 500 m of MgB_2 superconducting wire into a double pancake coil using the wet-winding technique. The coil is tested for contacts between the turns to evaluate the suggested one-step wet-winding process.

© 2015 The Authors. Published by Elsevier Ltd.
Selection and peer-review under responsibility of SINTEF Energi AS.

Superconductor generator; coil winding; electrical insulation

* Corresponding author. Tel.: +47 90718577; fax: +47 73597250.
E-mail address: niklas.magnusson@sintef.no

1876-6102 © 2015 The Authors. Published by Elsevier Ltd.
Selection and peer-review under responsibility of SINTEF Energi AS.

1. Introduction

To reduce the foundation and installation costs per unit generated energy, off-shore wind turbines with power ratings of 10 MW and beyond are considered. New and innovative solutions are sought for every part of the construction of this next generation of wind turbines to reduce weight, volume and particularly cost.

For the generator, converting kinetic energy to electric energy, novel design features may be viable [1]. One of the new solutions considered for direct drive generators is the use of superconducting material in the generator field winding [2,3]. Under dc operation, superconductors carry current loss-free when cooled down to low temperatures, typically 4 - 40 K depending on the choice of superconductor. One main advantage is that the magnetic field can be considerably higher, a factor of two or more, than in copper coil or permanent magnet based generators. In this way the necessary torque can be realized within a much smaller volume in the superconducting generator than in its conventional counterparts. The volume and weight reductions achieved in this way may have a significant economical value, particularly for wind turbines at depths requiring floating platforms.

There are several superconductors considered for wind power generator windings, operating at various temperatures and magnetic fields, and available at different cost [4]. Operating at 4 K, the low-temperature superconductor, NbTi, extensively used in MRI machines, constitutes a proven magnet technology. One path may be to transfer this technology into the wind turbine [5]. Another path may be to employ the high-temperature superconductor YBCO at temperatures of 40 -50 K [6]. A third option is the superconductor MgB_2 operating at the intermediate temperatures of 15 - 20 K [7,8]. In this temperature interval, the current density of the wire at a magnetic field of 2 T is presently 100 - 200 A/mm^2 (25 – 50 times higher than in copper conductors) for commercially available wires [8]. The present wire cost is approximately 20 €/kAm, which is one fifth to one third of the cost for copper conductors. The MgB_2 conductor is still under development and an enhanced performance together with gains from up-scaling of production are expected to lead to a further cost reduction. Among the negative aspects on superconductor technology is the cost for cooling and cryogenic equipment, which also needs to be included in the economical assessment.

In the European project INNWIND.EU [9] generators based on two of these superconductors, YBCO and MgB_2, are investigated. In the present work we focus on the fabrication of superconducting windings based on MgB_2 superconductors. The principles of the winding technique are outlined and special attention is paid to the turn-to-turn electrical insulation.

Superconducting windings are normally impregnated with epoxy and can either be dry-wound or wet-wound. In the dry-winding method the conductor is insulated typically with a glass-fibre fabric, then wound into the coil and afterwards vacuum impregnated with an epoxy [10]. In the wet-winding method the conductor is typically insulated with a polymer foil (e.g. Kapton) and then wound while applying a thin layer of epoxy to the conductor sides [11].

In recent years, non-insulated coils (i.e. without turn-to-turn insulation) have gained significant interest for high-temperature superconducting coils [12,13,14,15]. There are several benefits with non-insulated coils, such as increased compactness and thereby increased overall current density, enhanced thermal stability at quench situations, overall high thermal conductivity of the coil, and avoidance of the so called spongy effect [16] due to differences in Young's modulus between the polymeric insulation and the conductor.

One disadvantage with non-insulated coils is the prolonged ramping time due to the presence of induced currents between turns at high ramping rates. The problem may be reduced or eliminated by the use of a partial insulation between the turns (using a poor conductor between turns or insulating only parts of the windings), thereby increasing the turn-to-turn resistance and allowing for an increased ramping rate [17,18]. Another disadvantage, for coils such as generator rotors which are operated in the presence of a low ac magnetic field, is that such fields, similarly to the situation during ramping, may induce unwanted ac currents in the coil through turn-to-turn contacts.

In this work we investigate the possibility to use the wet-winding technique without any dedicated electrical insulation except for the epoxy applied to the conductor during winding. In principle, the epoxy gives a sufficiently thick layer for electrical insulation [19], however the method needs to be proven and the resistance of possible contact spots needs to be determined and their effect on the coil operation to be evaluated.

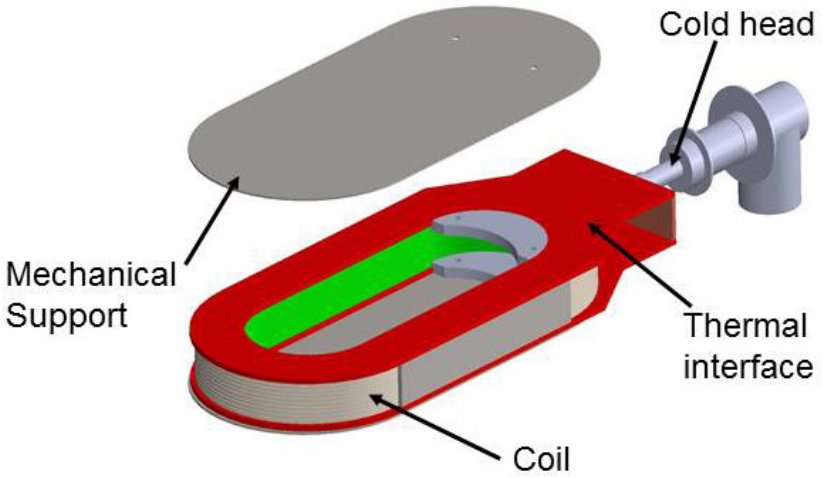

Fig. 1. Sketch of the MgB_2 demonstrator coil with thermal interface and mechanical support (to be mounted on the thermal interface).

2. The INNWIND.EU MgB_2 pole demonstrator

To evaluate the feasibility of superconducting MgB_2 generators a 10 MW generator is being designed [8]. The generator has 32 poles, and a key element is the superconducting coil itself. In the 10 MW design the race-track shaped coil has a straight section of 2.8 m and two end sections with inner radii of 0.15 m. The cross-section of the coil is 84 mm x 80 mm (width x height), the number of turns 200, and the current 235 A. The maximum magnetic field is 3 T, appearing at the inner part of the end sections.

The INNWIND.EU MgB_2 pole demonstrator has the same features except for that the straight section is made considerably shorter (0.5 m) to fit the coil into an existing test facility and to reduce the wire cost. The main objective for the coil demonstration is to evaluate the feasibility of a one-step wet-winding technique and the ability of such a coil to handle the thermal contraction and the large Lorentz forces appearing under operation. Figure 1 shows the coil with thermal interface, mechanical support and the cold head of the cryocooler.

3. Winding race-track coils

MgB_2 superconductors are currently produced in lengths of one to a few kilometres. This is less than what is required for the coil in the 10 MW design. A commonly used method to allow for well controlled splices is to wind so called double pancake coils. The winding procedure starts with the mid part of a wire length, which crosses between a lower and an upper pancake. Half of the wire length is then wound into a lower layer pancake and afterwards the remaining half is wound into an upper layer pancake. In this way the wire ends appear at the outside of the coil and are easily spliced to neighbouring double pancake coils in a low magnetic field and easily cooled region.

The wet-winding technique is previously successfully used to wind round double pancake MgB_2 coils [11]. Figure 2 shows the winding table adjusted for winding of race-track coils. To the left the lower layer of the double pancake is wound while the wire for the second half is placed in the spool at the top of the rotating table. In the right hand figure, the second layer is wound. Spacers about 0.5 mm thick (not seen because of the black epoxy) are placed at a few locations around the winding to ensure a space filled with epoxy constituting the electrical insulation between the layers. The epoxy used is the alumina filled Stycast 2850.

Fig. 2. Winding table during winding of the first layer (left) and second layer (right) of a double pan-cake MgB_2 coil.

4 Turn-to-turn insulation

4.1 Need for turn-to-turn insulation

In principal, during pure dc operation of a superconducting coil, no turn-to-turn insulation would be necessary. The current is carried loss-free and consequently no voltages would appear between turns, and the current flows only in the superconducting filaments of the wire. However, this is not the case for a coil under real operation. First, the flux flow losses appearing below (but close to) the critical current of the conductor give rise to a small dc voltage over a coil turn. Second, during ramping of the coil, the enclosed flux within the coil changes and consequently a turn-to-turn voltage is induced. If the ramping rate is constant, this voltage is a dc voltage. Thirdly, in a practical wind turbine generator rotor, ac magnetic fields are present leading to induced ac voltages in the rotor winding.

Figure 3 shows a cross-section of a test winding. The epoxy layer applied in the wet-winding process constitutes an effective electrical insulation as long as there are no spots incidentally left dry during the wetting process or that the pressure during winding has squeezed the epoxy away at certain points. The uneven top layer is due to long winding time at this first trial winding leading to problems finishing within the pot life of the epoxy. Nevertheless, the test winding can be used to estimate the quality of the epoxy as electrical insulation in the coil.

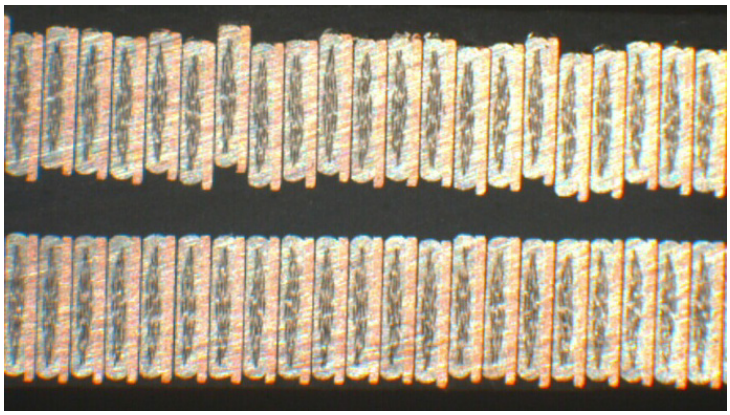

Fig. 3. Cross-section of a part of the MgB_2 double pancake test coil. In this cross-section, the microscope picture shows that a sufficiently thick layer of epoxy has been applied. The width of the MgB_2 wire is 3 mm.

4.2 Turn-to-turn voltages appearing under operation

Under steady operation, the dc electric field, E_{dc}, along a superconductor operated in the flux-flow region, i.e. relatively close to its critical current, normally follows a power-law dependence according to:

$$E_{dc} = E_0 \left(\frac{I}{I_c} \right)^n , \tag{1}$$

Where E_0 is 1 x 10^{-4} V/m, I is the current in the superconductor, I_c is its in-field critical current, and n is an empirically determined exponent. For an MgB_2 wire operated at a safety margin of 25% and with a typical n-value of 20, E becomes 0.3 μV/m. For one turn in the 10 MW generator rotor coil the voltage then becomes 2 μV since the length of the turn is 6.6 m.

During current ramping, the voltage over the entire coil, U_{coil}, is determined by:

$$U_{coil} = L \frac{dI}{dt}, \tag{2}$$

where L is the coil inductance. The inductance of the field winding for the 10 MW generator rotor coil is around 10 H and a typical ramping rate is 0.1 A/s, energizing the coil in 40 minutes. The total coil voltage then becomes 1 V and with 200 turns in the coil, the average voltage for one turn becomes 5 mV. Although varying with position in the coil (somewhat higher at the inner turns and lower at the outer turns) this is the order of magnitude of the turn-to-turn voltage during current ramping.

The space distribution of the magnetic field in the air-gap of the machine contains a fundamental component (sinusoidal distribution) and several harmonics. The harmonics spectrum depends on the design of the rotor and stator. For a stator winding comprising slots and teeth, the harmonic spectrum depends on the number of slots per pole and per phase (q), and if the teeth are magnetic or not. The amplitude of the harmonics becomes larger with magnetic teeth.

When the number of slots per pole and phase q is an integer number, only over-harmonic components are present in the air gap field. They may cause losses in the superconducting field winding if the winding is insufficiently shielded. However, the net flux change and hence the induced voltage in the field winding is small due to the short wavelength of the over-harmonics.

In case of a fractional winding in the stator (e.g. q=1.5), there are sub-harmonic components in the magnetic field spanning several poles. They can create a net flux in field winding leading to an ac voltage in the winding. The sub-harmonics can however be reduced by a proper selection of the number of slots in the machine. In addition the frequency is low such that the induced voltage is usually no problem.

To get one estimation of the turn-to-turn voltage we may use the magnetic field distribution in [21] calculated for a superconducting generator with non-magnetic teeth. The dominating harmonic frequency in that design is 10 Hz and the (rms) magnetic flux density approximately 3 mT. Now, as this field varies spatially several times over the enclosed area of the field coil, the net flux is maybe one fifth of the area times the magnetic field. The voltage for one turn can then be estimated by,

$$U_{turn} = \frac{d\phi}{dt}, \tag{3}$$

where Φ is the enclosed magnetic flux (equal to the magnetic field times the area). With a total area of the field winding in the 10 MW design of 1 m^2, the turn voltage becomes approximately 40 mV. It should be noted that this

is a very rough estimate only used to get the order of magnitude of the turn-to-turn voltage that could be appearing in the field winding.

Summarizing the turn-to-turn voltages they are of the order 2 μV, 5 mV and 40 mV for the dc operation, ramping and ac harmonics, respectively.

4.3 Turn-to-turn resistance in the double pancake test coil

The double pancake test coil was fed by a dc current of 1 A in room temperature and voltages were measured over approximately one quarter, half, three quarters and the full coil to 1.12, 2.47, 3.58 and 5.04 V, respectively. These numbers reveal no large differences between the quarters of the coil and correspond to the anticipated voltage drops in the wire without large currents passing between turns (and certainly not between the lower and upper layers). It should be noted, though, that the resistance along one turn of the test coil is only about 25 mΩ and for differences in voltages to be detected in these initial measurements, the turn-to-turn resistance needs to approach this level.

To obtain more accurate values on the possible turn-to-turn contact resistance, the coil was cut into four parts and the ends of these parts were sanded (figure 3). The resistances between turns were measured directly (under microscope) using an ohm-meter for values above and a four point method for values below 1 Ω. Several contact point were then detected without any visible contacts at the ends even in the microscope. However, a contact point of the order 1 Ω can be very small and is generally determined by:

$$d = \frac{\rho}{R}, \tag{4}$$

where d is the diameter of the contact point, ρ the resistivity of the contact materials (in this case a mixture of copper and nickel) and R the contact resistance. With ρ of the order 2 x 10^{-8} Ωm and the resistance of the order 1 Ω, the diameter of the contact spot becomes approximately 0.02 μm which is less than what can be seen in a microscope. To eliminate possible contacts at the sanded surfaces, 10 V was applied between turns to burn out any conducting material constituting the contact. For all resistances below 1 Ω the method was effective and sparks could be seen from one of the ends on all samples, showing that the contacts were located at the surfaces (and most likely created during cutting or sanding) and not within the actual coil. For contact resistances above a few Ω the applied voltage had no effect.

In contrast to the low resistance values which were somewhat fluctuating, there were a number of high and stable turn-to-turn resistances. It is likely to believe that these values, which were of the order tens of Ω to several kΩ, are in fact contacts between turns. Their cause may be small particles within the epoxy, imperfections in or metal rest from the wire, or simply that a too thin layer of epoxy was applied, particularly in the second layer of the double pancake test coil where the layers tended to position in an uncontrolled manner.

4.4 Influence of currents possibly passing the contact points

Taking the maximum turn-to-turn voltage from section 4.2 (40 mV) and the minimum resistance from section 4.3 (10 Ω) the current passing the worst contacts can be estimated at 4 mA. This current is far less than the 0.1% of the dc current acceptable from the ac loss point of view [20]. Another question is the power dissipated locally, in this case 0.2 mW, at the contact spot. However, the heat is not generated directly in the superconducting filaments but at the metal surface. The thermal conductivity of the materials will ensure that the heat is conducted both along the wire and through the thin epoxy layer towards the inside of the coil where it is cooled. In fact, if one considers that the heat is conducted in 1 square centimetre from the outermost turn to the inside of the coil, the 0.2 mW corresponds to a temperature increase of only approximately 2 mK.

4. Conclusion

Using the epoxy itself as electrical insulation in the wet-winding technique may be a viable and attractive method when winding superconducting coils. A test wound coil showed no low resistive contacts, and it is likely that an all through well controlled winding process would increase any contact resistances further. By avoiding a dedicated electrical insulation, like Kapton, the cost is reduced (the insulation cost is about 10% of the cost of the MgB_2 wire), one step in the coil manufacturing process is removed, and maybe most importantly, the radial thermal conductivity of the coil increases dramatically.

Acknowledgements

This work is part of the NOWITECH programme supported by the Research Council of Norway, and of the INNWIND.EU project supported by the Seventh Framework Programme (FP7) under Grant Agreement No. 308974.

References

[1] Zhang Z, Chen A, Matveev A, Nilssen R, Nysveen A. High-power generators for offshore wind turbines. Energy Procedia, 2013;35: 52-61.
[2] Abrahamsen AB, Mijatovic N, Seiler E, Zirngibl T, Træholt C, Nørgård PB, Pedersen NF, Andersen NH Østergård J. Superconducting wind turbine generators. Supercond Sci Technol 2010;23:034019.
[3] Fukui S, Ogawa J, Takao S, Tsukamoto O, Kashima N, Nagaya S. Study of 10 MW-Class Wind Turbine Synchronous Generators With HTS Field Windings. IEEE Trans Appl Supercond 2011;21:1151-4.
[4] Abrahamsen AB, Magnusson N, Jensen BB, Runde M. Large superconducting wind turbine generators. Energy Procedia 2012;24:60-7.
[5] Fair R, Stautner W. Superconductivity for large scale wind turbines. DOE report 2012.
[6] Schacherer C, Kraemer HP, Kuhnert A, Oomen M, van Hasselt P, Frank M. Basic investigations of a 2G high-temperature superconducting race track coil for wind power applications. Presented at Applied Superconductivity Conference, Charlotte, USA. 10-15 August 2014.
[7] Apiñániz S, Arlaban T, Manzanas R, Tropeano M, Funke R, Kovác P, Yang Y, Neuman H, Duluc X, Sanz S. Superconducting light generator for large offshore wind turbines. J Phys Conf Ser 2014;507:032040.
[8] Abrahamsen AB, Magnusson N, Jensen BB, Liu D, Polinder H. Design of an MgB_2 race track coil for a wind generator pole demonstration. J Phys Conf Ser 2014;507:032001.
[9] www.innwind.eu (9 January 2015)
[10] Modica M, Angius S, Bertora L, Damiani D, Marabotto M, Nardelli D, Perrella M, Razeti M, Tassisto M. Design, construction and tests of MgB_2 coils for the development of a cryogen free magnet. IEEE Trans Appl Supercond 2007;17:2196-9.
[11] Sætre F, Hiltunen I, Runde M, Magnusson N, Järvelä J, Bjerkli J, Engebrethsen E. Winding, cooling and initial testing of a 10 H superconducting MgB_2 coil for an induction heater, Supercond Sci Technol 2011; 24:035010.
[12] Hahn S, Park DK, Bascuñán J, Iwasa Y. HTS pancake coils without turn-to-turn insulation. IEEE Trans Appl Supercond 2011;21;1592-5.
[13] Hahn S, Song J, Kim Y, Lecrevisse T, Chu Y. Voccio J, Bascunan J, Iwasa Y. Construction and Test of 7-T/68-mm Cold-Bore Multiwidth No-Insulation GdBCO Magnet. IEEE Trans Appl Supercond 2015;25:4600405.
[14] Park H, Kim A, Kim S, Park M, Kim K, Park T. Mechanical and electric characteristics of vacuum impregnated no-insulation HTS coil. Physica C 2014;504:138-43.
[15] Kwon OJ, Kim KL, Choi YH, Shin HJ, Hahn S, Iwasa Y, Lee HG. Effects of turn-to-turn compactness in the straight sections of HTS racetrack coils on thermal and electrical characteristics. Supercond Sci Technol 2013;26:085025.
[16] Wilson MN. Superconducting magnets. New York:Oxford University Press 1983, p. 46.
[17] Choi YH, Kim KL, Kwon OJ,Kang DH, Kang JS, Ko TK, Lee HG. The effects of partial insulation winding on the charge–discharge rate and magnetic field loss phenomena of GdBCO coated conductor coils. Supercond Sci Technol 2012;25:105001
[18] Lee TS, Hwang YJ, Lee J, Lee WS, Kim J, Song SH, Ahn MC, Ko TK. The effects of co-wound Kapton, stainless steel and copper, in comparison with no insulation, on the time constant and stability of GdBCO pancake coils. Supercond Sci Technol 2014;27:065018.
[19] Runde M, Stenvall A, Magnusson N, Grasso G, Mikkonen R. MgB_2 coils for a DC superconducting induction heater. J Phys Conf Ser 2008:97;012159.
[20] Magnusson N, Abrahamsen AB, Liu D, Runde M, Polinder H. Hysteresis losses in MgB_2 superconductors exposed to combinations of low AC and high DC magnetic fields and transport currents. Physica C 2014;506:133-7.
[21] Schellevis J. AC Loss Modelling of Superconducting Field Windings for a 10MW Wind Turbine Generator. TU Delft, master of ccience thesis 2014, p.40.